TWEAK modulates the characteristics of periodontal ligament stem cells via the Fn14/NF-κB pathway

LINLIN XIAO[1,2*], MAN QU[1,2*], LULU CHEN[1,2*], MINGLI XIANG[1,2], QIAN LONG[1,2], JIANGUO LIU[2], XIAOYAN GUAN[1,2] and CHENGCHENG LIAO[1-3]

[1]Department of Orthodontics II, Affiliated Stomatological Hospital of Zunyi Medical University, Zunyi, Guizhou 563000, P.R. China; [2]Oral Disease Research Key Laboratory of Guizhou Tertiary Institution, School of Stomatology, Zunyi Medical University, Zunyi, Guizhou 563000, P.R. China; [3]West China School of Stomatology, Sichuan University, Chengdu, Sichuan 610041, P.R. China

Received March 28, 2025; Accepted September 4, 2025

DOI: 10.3892/ijmm.2025.5679

Abstract. Tumor necrosis factor-like weak inducer of apoptosis (TWEAK)/fibroblast growth factor-inducible 14 (Fn14) signaling represents a critical regulatory axis in tissue repair and the inflammatory response. However, the impact of TWEAK on the characteristics of periodontal ligament stem cells (PDLSCs), which subsequently influence periodontal homeostasis, remains inadequately understood. To address this, PDLSCs were isolated from human periodontitis tissue and cultured to investigate the effects of TWEAK on PDLSC proliferation, migration and osteogenic differentiation using Cell Counting Kit-8, TUNEL, Transwell and scratch assays, and alizarin red and alkaline phosphatase staining. Transcriptome sequencing and western blot analysis were used to explore the underlying molecular mechanisms. Additionally, the potential of targeting TWEAK in periodontitis treatment was evaluated using inflammatory PDLSCs (iPDLSCs) and a rat periodontitis model. The present study demonstrated that low levels (1, 5 and 20 ng/ml) of TWEAK enhanced the proliferation and osteogenic differentiation of PDLSCs, with 1 and 5 ng/ml further enhancing their ability to promote M2 macrophage polarization. By contrast, elevated levels (100 ng/ml) of TWEAK impaired PDLSC proliferation, migration and osteogenic potential, activated the RANKL/osteoprotegerin (OPG) system, and promoted the M1 polarization of macrophages induced by PDLSCs, with the Fn14/NF-κB pathway serving a pivotal role in this regulatory process. The expression levels of TWEAK, Fn14 and NF-κB were significantly higher in iPDLSCs than in healthy donor-derived PDLSCs, and these iPDLSCs exhibited reduced proliferation, migration and osteogenic potential, along with increased RANKL/OPG activation and M1 macrophage polarization. In iPDLSCs, inhibition of the TWEAK/Fn14/NF-κB pathway enhanced cell proliferation, migration and osteogenic differentiation potential, and reversed the activation of the RANKL/OPG system and macrophage M1 polarization induced by iPDLSCs. Furthermore, high TWEAK levels were shown to accelerate the progression of rat periodontitis, while inhibition of the TWEAK/Fn14 pathway mitigated periodontitis-induced periodontal tissue destruction in rats. Collectively, the present findings revealed the role of the TWEAK-PDLSCs axis in the maintenance and disruption of periodontal homeostasis, and identified targeting of the TWEAK/Fn14/NF-κB pathway in iPDLSCs during periodontitis as a promising therapeutic strategy.

Correspondence to: Dr Chengcheng Liao or Professor Xiaoyan Guan, Department of Orthodontics II, Affiliated Stomatological Hospital of Zunyi Medical University, 201 Dalian Road, Zunyi, Guizhou 563000, P.R. China
E-mail: lcc_950330@163.com
E-mail: 1278279125@qq.com

*Contributed equally

Key words: tumor necrosis factor-like weak inducer of apoptosis, fibroblast growth factor-inducible 14, periodontal ligament stem cells, NF-κB, periodontal, periodontitis

Introduction

Tumor necrosis factor (TNF)-like weak inducer of apoptosis (TWEAK) and its homologous receptor, fibroblast growth factor-inducible 14 (Fn14), are members of the TNF superfamily (1). TWEAK is widely expressed in monocytes, dendritic cells and natural killer cells, with macrophages and monocytes representing the principal sources of soluble TWEAK in inflamed tissues (2). Fn14 is expressed in various nonhematopoietic cells, including epithelial, endothelial, astrocytic, cancer, keratinocyte, mesenchymal and neuronal cells (3-6). The TWEAK/Fn14 pathway serves pivotal roles in maintaining tissue homeostasis, facilitating repair after injury, and contributing to disease progression by influencing cellular proliferation, migration and angiogenesis, among other processes (7-9). Previous studies have shown that TWEAK expression is increased in periodontal tissues and gingival crevicular fluid from patients with periodontitis (10-12). However, the roles of TWEAK in periodontal homeostasis and the progression of periodontitis remain poorly understood.

The periodontium consists of the cementum, alveolar bone and periodontal ligament (PDL). Periodontal tissues undergo

continuous remodeling to maintain the integrity of these structures in response to stimuli such as microbial and mechanical forces (13,14). As periodontal inflammation progresses, it can lead to alveolar bone destruction, a loss of PDL attachment and eventual tooth loss, impairing the patient's ability to chew, speak and maintain self-esteem (15). The cellular components of the periodontium, particularly PDL stem cells (PDLSCs), serve crucial roles in both homeostasis and decompensation (16,17). PDLSCs are multipotent stem cells capable of self-renewal and differentiation into various cell types within the PDL, including osteoblasts, ligament cells and cementoblasts (18). Furthermore, PDLSCs exert immunoregulatory effects (19), influence osteoclast formation (20) and contribute to vascular remodeling (21) within the periodontal environment via paracrine signaling. Therefore, the present study aimed to investigate the influence of TWEAK on the characteristics of PDLSCs to elucidate its potential role in periodontal homeostasis and decompensation progression.

In the present study, human periodontitis tissue-derived PDLSCs [inflammatory PDLSCs (iPDLSCs)] were isolated and cultured to assess the impact of various TWEAK concentrations on PDLSC proliferation, migration and osteogenic differentiation. Co-culture techniques were further employed to evaluate the regulatory potential of TWEAK-pretreated PDLSCs on osteoclast and macrophage activity. Transcriptomic analysis, coupled with *in vitro* validation, was used to elucidate the specific molecular mechanisms by which TWEAK influences PDLSCs characteristics. Additionally, the efficacy of targeting the TWEAK-Fn14 pathway for the treatment of periodontitis was validated in both human periodontitis tissue-derived PDLSCs (iPDLSCs) and a rat periodontitis model.

Materials and methods

Cell culture and identification. A total of 16 healthy premolars or third molars extracted for orthodontic purposes (donor characteristics: Mean age ± SD, 18.75±0.77 years; range, 18-20 years; male-to-female ratio, 9:7) and six third molars from patients with periodontitis (donor characteristics: Median age, 19 years; range, 18-20 years; male-to-female ratio, 1:1) were obtained from the Affiliated Stomatological Hospital of Zunyi Medical University (Zunyi, China) between August 2023 and June 2025. The donors were systemically healthy and had not received any antibiotics or anti-inflammatory treatments within the preceding 2 weeks. All human tissue treatment protocols were approved by the Ethics Committee of the Affiliated Stomatological Hospital of Zunyi Medical University (approval no. ZYKQ-IRB-CT-2023-065; Zunyi, China), with written informed consent obtained from all participants. All samples were thoroughly rinsed with saline and incubated for 30 min at 4˚C in saline containing 100 U/ml penicillin-streptomycin (cat. no. 15140148; Gibco; Thermo Fisher Scientific, Inc.) prior to processing. The PDL tissue was scraped from the middle third of the tooth root surface, cut into small pieces and digested with collagenase I (cat. no. 9001-12-1; Beijing Solarbio Science & Technology Co., Ltd.) for 15 min at 37˚C. The cells were cultured in α-Minimum Essential Medium (α-MEM; cat. no. 12571063; Gibco; Thermo Fisher Scientific, Inc.) supplemented with 10% FBS (cat. no. 10099158; Gibco; Thermo Fisher Scientific, Inc.) and 100 U/ml penicillin-streptomycin (cat. no. 15140148; Gibco; Thermo Fisher Scientific, Inc.). PDLSCs from the third generation (P3) to fifth generation (P5) were used for flow cytometry, cell proliferation assays, osteogenic induction, cell migration assays, and the extraction of cellular RNA and proteins. RAW264.7 mouse monocyte macrophage cells were purchased from HyCyte® (Suzhou Haixing Biological) and cultured in RPMI 1640 medium (cat. no. 11875119; Gibco; Thermo Fisher Scientific, Inc.) supplemented with 10% FBS and 100 U/ml penicillin-streptomycin. Both PDLSCs and RAW264.7 cells were cultured at 37˚C, with 5% CO_2 and 100% humidity.

For the identification of surface protein expression in PDLSCs, adherent cells were resuspended in 0.25% trypsin-EDTA (cat. no. 25200114; Gibco; Thermo Fisher Scientific, Inc.) and incubated with CD44-FITC (cat. no. 555478; BD Biosciences), CD90-FITC (cat. no. 555595; BD Biosciences), CD105-FITC (cat. no. 561443; BD Biosciences), CD29-phycoerythrin (PE) (cat. no. 555443; BD Biosciences), CD73-PE (cat. no. 550257; BD Biosciences), CD11b-FITC (cat. no. 557396; BD Biosciences), CD31-FITC (cat. no. 555445; BD Biosciences), CD34-FITC (cat. no. 555821; BD Biosciences) and CD45-FITC (cat. no. 555482; BD Biosciences) antibodies in the dark at 4˚C for 60 min. Subsequently, surface marker expression was analyzed by flow cytometry (Beckman Cytomics™ FC 500; Beckman Coulter, Inc.). FlowJo v10.8.1 software (BD Biosciences) was used for the analysis and plotting of the flow cytometry results. In addition, images of primary cells scraped from PDL tissue and P1 PDLSCs were captured using a light microscope to observe the morphological characteristics of the PDLSCs.

PDLSCs were induced for adipogenic differentiation using the Human Adipogenic Differentiation Kit (cat. no. HUXXC-90021; Oricell; Cyagen Biosciences Co., Ltd.) according to the manufacturer's instructions. Cells were treated with Solution A for 3 days, followed by Solution B for 1 day, repeating this cycle five times under culture conditions of 37˚C with 5% CO_2 and 100% humidity. After induction, cells were fixed with 4% paraformaldehyde (cat. no. P1110; Beijing Solarbio Science & Technology Co., Ltd.) at room temperature for 15 min, stained with Oil Red O for 1 h at room temperature to visualize lipid droplets, and images of adipogenically differentiated PDLSCs were captured using a light microscope.

Cellular immunofluorescence staining. The cells were cultured in confocal dishes (cat. no. 801001; Wuxi NEST Life Science Co., Ltd.). After treatment with TWEAK or NF-κB signaling pathway inhibitor (NF-κB-IN-1), the cells were fixed with 4% paraformaldehyde (cat. no. P1110; Beijing Solarbio Science & Technology Co., Ltd.) for 15 min at room temperature. The cells were permeabilized with 0.5% Triton X-100 (cat. no. T8200; Beijing Solarbio Science & Technology Co., Ltd.) at room temperature for 15 min. Antigen retrieval was performed by incubation with 0.4% pepsin (cat. no. CR2304020; Wuhan Servicebio Technology Co., Ltd.) at 37˚C for 30 min. Subsequently, cells were blocked with 5% BSA (cat. no. SW3015; Beijing Solarbio Science & Technology Co., Ltd.) for 1 h at room temperature. The diluted primary antibodies (1:200) were applied to the samples and these were

incubated overnight at 4˚C. Fluorescent dye-conjugated antibodies, including Alexa Fluor 647-conjugated goat anti-rabbit (cat. no. A21244; Invitrogen; Thermo Fisher Scientific, Inc.) and Alexa Fluor 555-conjugated goat anti-mouse (cat. no. A21422; Invitrogen; Thermo Fisher Scientific, Inc.) antibodies, were diluted 1:400 and cells were incubated with these at room temperature for 30 min. The cell nuclei were stained with a DAPI solution (cat. no. C0065; Beijing Solarbio Science & Technology Co., Ltd.) at a 1:5,000 dilution at room temperature for 5 min. Images were captured using a confocal laser scanning microscope (Olympus FV1200 or Olympus VS200; Olympus Corporation). The primary antibodies used for immunofluorescence staining included the mouse anti-receptor activator of nuclear factor-κB ligand (RANKL) antibody (cat. no. sc-52950; Santa Cruz Biotechnology, Inc.), rabbit anti-osteoprotegerin (OPG) antibody (cat. no. ab73400; Abcam), mouse anti-CD68 antibody (cat. no. ab201340; Abcam) and rabbit anti-CD163 antibody (cat. no. ab182422; Abcam). ImageJ 1.8 (National Institutes of Health) was used to analyze the fluorescence intensity of the images.

TWEAK and NF-κB-IN-1. Recombinant human cynomolgus TWEAK/TNF superfamily member 12 (TNFSF12) protein (mFc tag) (cat. no. 90094-C04H; Sino Biological, Inc.) was dissolved in sterile water to obtain a stock solution concentration of 50 μg/ml. The stock solution was further diluted with α-MEM to 1, 5, 20, 50 and 100 ng/ml, respectively, and the resulting TWEAK solutions were used to stimulate the cells for 48-72 h at 37˚C. NF-κB-IN-1 (cat. no. HY-138537; MedChemExpress), a 4-aryl curcumin analog, is an effective inhibitor of the NF-κB signaling pathway. NF-κB-IN-1 directly inhibits IKK, thus blocking the activation of NF-κB (22). PDLSCs were pretreated with 5 μM NF-κB-IN-1 for 4 h at 37˚C and then cultured in α-MEM for 48-72 h at 37˚C before western blot analysis.

Cell proliferation, apoptosis and colony formation assays. A Cell Counting Kit-8 (CCK-8) (cat. no. C0038; Beyotime Institute of Biotechnology) was used to assess cell proliferation. The cells were incubated with CCK-8 reagent for 1 h, and the absorbance at 450 nm was measured using a microplate reader (Thermo Fisher Multiskan FC; Thermo Fisher Scientific, Inc.) to evaluate proliferation.

A One Step TUNEL Apoptosis Assay Kit (cat. no. C1088; Beyotime Institute of Biotechnology) was used to detect apoptosis. Following the provided protocol, cells were fixed with 4% paraformaldehyde (cat. no. P1110; Beijing Solarbio Science & Technology Co., Ltd.) at room temperature for 15 min and permeabilized with 0.3% Triton X-100 (cat. no. T8200; Beijing Solarbio Science & Technology Co., Ltd.) at room temperature for 5 min. Subsequently, cells were incubated with the prepared EdUTP labeling solution at 37˚C for 60 min, followed by incubation with the Click reaction mixture for 30 min at room temperature in the dark, during which apoptotic cells were labeled with the green fluorescent probe fluorescein (FITC). Finally, the nuclei were stained with DAPI solution (1:5,000 dilution; cat. no. C0065; Beijing Solarbio Science & Technology Co., Ltd.) for 5 min at room temperature. The cells were washed with PBS for 5 min at room temperature before and after each step, repeated three times. Subsequently, after the cells were mounted with an antifade mounting medium (cat. no. S2110; Beijing Solarbio Science & Technology Co., Ltd.), fluorescence images were captured using a confocal laser scanning microscope (Olympus FV1200; Olympus Corporation). A total of five random images were acquired for each sample, and the mean positive rate was calculated for statistical analysis, with six samples per group.

The colony formation experiment involved inoculating 200 individual PDLSCs into each well of a six-well plate. After culturing the cells in complete medium for 2 weeks, they were fixed with 4% paraformaldehyde (cat. no. P1110; Beijing Solarbio Science & Technology Co., Ltd.) at room temperature for 15 min, followed by staining with crystal violet (cat. no. C8470; Beijing Solarbio Science & Technology Co., Ltd.) at room temperature for 30 min. The cells were then washed thoroughly with PBS and air-dried, and colony images were captured using a light microscope and DSLR cameras. A colony was defined as a cluster containing >50 PDLSCs.

Transwell migration and cell scratch wound healing experiments. The Transwell migration and cell scratch wound healing assays were used to assess cell migration. After 48-72 h of treatment with TWEAK or NF-κB-IN-1, or >48 h post-transfection, PDLSCs ($2x10^5$) diluted in serum-free α-MEM were seeded into the upper chamber of the Transwell insert (cat. no. 3422; Corning, Inc.), while the lower chamber contained α-MEM supplemented with 10% FBS. After 24 h of incubation at 37˚C, the cells on the pore membrane of the Transwell insert were fixed with 4% paraformaldehyde (cat. no. P1110; Beijing Solarbio Science & Technology Co., Ltd.) at room temperature for 15 min, and the cells on the upper side of the membrane were thoroughly washed with PBS. Subsequently, the cells on the lower side of the Transwell membrane were stained with crystal violet (cat. no. C8470; Beijing Solarbio Science & Technology Co., Ltd.) at room temperature for 30 min, and the number of cells that had migrated through the membrane was counted and recorded under a light microscope.

For the wound healing assay, $5x10^5$ PDLSCs, treated with TWEAK or NF-κB-IN-1 for 48-72 h or >48 h post-transfection, were seeded into each well of a 12-well plate to achieve >90% confluence after 24 h. Subsequently, a wound was mechanically created using a 200-μl pipette tip in the well of a plate to prevent the cells on both sides from coming into contact. The cells were washed with PBS and then cultured in serum-free α-MEM. Images of the same scratch wound area were captured under a light microscope at 0 and 24 h. ImageJ 1.8 (National Institutes of Health) was used to calculate the percentage of wound reduction in the same area between 0 and 24 h to compare the migration rates of cells on both sides of the wound toward the cell-free area.

Osteogenesis induction, Alizarin red staining and alkaline phosphatase (ALP) staining. The osteogenic induction solution was prepared according to the instructions provided with the Human Related Stem Cell Osteogenic Induction Differentiation Kit (cat. no. HUXXC-90021; Oricell; Cyagen Biosciences Co., Ltd.). When the cell confluence in the well plate reached 70%, the α-MEM was replaced with osteogenic induction medium, and the medium was changed every 3 days

thereafter. After 14-21 days of osteogenic induction, the cells were fixed with 4% paraformaldehyde at room temperature for 15 min, and mineralized nodules were stained with Alizarin Red S (pH 5.1-5.3) (cat. no. ALIR-10001; Oricell; Cyagen Biosciences Co., Ltd.) at 37˚C for 30 min. During the ALP staining experiment, the cells were subjected to 6-9 days of osteogenic induction. The cells were fixed with 4% paraformaldehyde at room temperature for 15 min, followed by staining with a BCIP/NBT Alkaline Phosphatase Staining Kit (cat. no. C3206; Beyotime Institute of Biotechnology) at 37˚C for 45 min to detect endogenous ALP. A light microscope was used to capture images of Alizarin Red and ALP staining, and ImageJ 1.8 (National Institutes of Health) was used for image processing.

Coculture of macrophages with PDLSCs. A Transwell coculture system (cat. no. 3412; Corning, Inc.) was used, with $1x10^6$ pretreated PDLSCs or iPDLSCs seeded in the upper chamber and $5x10^5$ macrophages cultured in the lower chamber. After 2 days of coculture, the cells from the lower chamber were harvested for the immunofluorescence analysis as aforementioned.

RNA-sequencing analysis. Total RNA was extracted from PDLSCs using TRIzol reagent (cat. no. 15596026CN; Invitrogen; Thermo Fisher Scientific, Inc.). Transcriptome sequencing was subsequently performed by Gene Denovo Co., Ltd. RNA integrity was assessed using the Agilent 2200 Tapestation (cat. no. G2965AA; Agilent Technologies, Inc.), with each sample exhibiting an RNA integrity number equivalent of ≥7.0. mRNA was isolated from total RNA and fragmented into ~200 bp fragments prior to cDNA synthesis. Library preparation was performed using the TruSeq RNA LT Sample Prep Kit (cat. no. RS-122-2001; Illumina, Inc.) for adapter ligation and low-cycle PCR enrichment. The purified library products were evaluated using the Agilent 2200 Tapestation and Qubit 2.0 (Thermo Fisher Scientific, Inc.), and then diluted to 10 pM. Sequencing was performed using the HiSeq 3000 platform (Illumina, Inc.), with paired-end sequencing (2x150 bp) on a HiSeq 3000 paired-end flow cell, according to the manufacturer's protocol. Sequencing was carried out using the HiSeq 3000 SBS Kit (cat. no. FC-401-3001; Illumina, Inc.).

Bioinformatics analysis was performed using the Omicsmart cloud bioinformatics platform (https://www.omicsmart.com/#/). Briefly, the quality of the raw reads was first evaluated using FastQC (v0.11.9; https://www.bioinformatics.babraham.ac.uk/projects/fastqc/). Low-quality reads and adapters were trimmed using Trimmomatic (v0.39; http://www.usadellab.org/cms/index.php?page=trimmomatic) with default parameters. The high-quality reads were then mapped to the reference genome (human, GRCh38; https://genome.ucsc.edu/) using HISAT2 (v2.2.1; https://daehwankimlab.github.io/hisat2/) with default settings. The resulting BAM files were sorted and indexed using SAMtools (v1.10; http://www.htslib.org/). Differential gene expression analysis was performed using the DESeq2 package (v1.30.0; https://bioconductor.org/packages/release/bioc/html/DESeq2.html) in R (v4.3.0; https://www.r-project.org/) (23). Gene counts were normalized using the DESeq2 method, and differential expression was determined using a negative binomial distribution model. Genes with an adjusted P-value <0.05 and a $\log_2$ fold change >1 or <-1 were considered significantly differentially expressed. Gene Ontology (GO) and Kyoto Encyclopedia of Genes and Genomes (KEGG) pathway enrichment analyses were performed using the clusterProfiler package (v3.18.1; https://www.bioconductor.org/packages/release/bioc/html/clusterProfiler.html?utm/) in R. GO enrichment analysis was conducted across all three categories, including biological processes, molecular functions and cellular components. For KEGG analysis, pathways were considered significantly enriched with a P-value <0.05. Enrichment results were visualized using bubble plots.

Short hairpin RNA (shRNA/sh)Fn14 and sh-NOD-like receptor thermal protein domain-associated protein 3 (NLRP3) lentiviral construction, and cell transfection. Lentiviral plasmids encoding shFn14 and shNLRP3 [contract nos. HYKY-230106022-DLV and HYKY-250428041-DLV; OBiO Technology (Shanghai) Corp., Ltd.] were packaged using a third-generation lentiviral system. 293T cells (cat. no. CRL-3216; American Type Culture Collection) were maintained at 37˚C in a humidified atmosphere containing 5% CO_2 and used as the packaging cell line. For transfection, 20 μg lentiviral transfer plasmid (cat. no. 10879; Addgene, Inc.), 15 μg packaging plasmids (psPAX2; cat. no. 12260; Addgene, Inc.) and 10 μg envelope plasmid (pMD2.G; cat. no. 12259; Addgene, Inc.) were co-transfected at a ratio of 2:1.5:1 using Lipofectamine 3000 (cat. no. L3000008; Thermo Fisher Scientific, Inc.) at 37˚C. Viral supernatants were collected 48 and 72 h post-transfection at 4˚C, filtered through a 0.45-μm filter at room temperature, and concentrated by ultracentrifugation at 50,000 x g for 2 h at 4˚C. The average viral titer of the constructs was $2.99x10^8$ TU/ml. The MOI for PDLSCs transfected with lentivirus was set at 30, and the calculation formula was as follows: Multiplicity of infection=virus titer (TU/ml) x virus volume (ml)/cell number. The lentivirus was combined with 1 mg/ml Polybrene Plus [cat. no. PTSJ-GR001; OBiO Technology (Shanghai) Corp., Ltd.] in serum-free and antibiotic-free α-MEM, and the mixture was used to infect the cells for 24 h at 37˚C, after which they were cultured in complete medium at 37˚C for continued growth. After 48-72 h, 0.5 mg/ml puromycin dihydrochloride (cat. no. ST551-10 mg; Beyotime Institute of Biotechnology) was used to eliminate unsuccessfully transfected cells for 48 h, and western blot analysis was performed to assess the transfection efficiency. Transfected cells were used for two passages, and to avoid potential effects of puromycin dihydrochloride on the proliferation, migration and differentiation capacity of PDLSCs, puromycin dihydrochloride was not included in subsequent cultures. Subsequently, the transfected cells were maintained in complete medium. The target sequences for the shRNAs used in the present study were as follows: sh-negative control, 5'-TTCTCCGAACGTGTCACGT-3'; sh-Fn14-1, 5'-AGGAGAGAGAAGTTCACCACC-3'; sh-Fn14-2, 5'-ACCTGGACAAGTGCATGGACT-3'; sh-Fn14-3, 5'-TCTGAGCCTGACCTTCGTGCT-3'; sh-NLRP3-1, 5'-GTGGATCTAGCCACGCTAATG-3'; sh-NLRP3-2, 5'-CCGTAAGAAGTACAGAAAGTA-3'; and sh-NLRP3-3, 5'-GCGTTAGAAACACTTCAAGAA-3'.

RT-qPCR. Total RNA was extracted from human PDLSCs using the FastPure Cell/Tissue Total RNA Isolation Kit V2 (cat. no. 7E730G3; Vazyme Biotech Co., Ltd.) at 4˚C. Following the normalization of the RNA concentration, the mRNA was reverse transcribed into cDNA using the HiScript III RT SuperMix for qPCR (+gDNA wiper) kit (cat. no. R323-01; Vazyme Biotech Co., Ltd.) under the following conditions: 25˚C for 5 min, 42˚C for 30 min and 85˚C for 5 min to inactivate the reverse transcriptase. Subsequently, relative qPCR analysis was conducted using the Taq Pro Universal SYBR qPCR Master Mix Kit (cat. no. Q712-02; Vazyme Biotech Co., Ltd.) on the QuantStudio 6 Flex Real-Time PCR System (Thermo Fisher Scientific, Inc.) under the following PCR conditions: Initial denaturation at 95˚C for 5 min, followed by 40 cycles of 95˚C for 10 sec and 60˚C for 30 sec, with fluorescence acquisition during the annealing/extension step. The data were analyzed using the $2^{-\Delta\Delta Cq}$ method (24) to quantify relative mRNA levels, with β-actin serving as the internal control. The primers used were synthesized by Sangon Biotech Co., Ltd. The specific sequences of primers used were as follows: Runt-related transcription factor 2 (RUNX2) forward, 5'-CTTTACTTACACCCCGCCAGTC-3' and reverse, 5'-AGAGATATGGAGTGCTGCTGGTC-3'; OPG forward, 5'-CTGGAACCCCAGAGCGAAAT-3' and reverse, 5'-GCGTTTACTTTGGTGCCAGG-3'; ALP forward, 5'-TAAGGACATCGCCTACCAGCTC-3' and reverse, 5'-TCTTCCAGGTGTCAACGAGGT-3'; Sp7 transcription factor (SP7) forward, 5'-CCTCTGCGGGACTCAACAAC-3' and reverse, 5'-AGCCCATTAGTGCTTGTAAAGG-3'; and β-actin forward, 5'-CAGCCTTCCTTCCTGGGCATG-3' and reverse, 5'-ATTGTGCTGGGTGCCAGGGCAG-3'.

Western blotting. The cells were lysed using RIPA lysis buffer (cat. no. P0013B; Beyotime Institute of Biotechnology) supplemented with 1 mM PMSF (cat. no. ST2573-5g; Beyotime Institute of Biotechnology), and whole-cell protein lysates were obtained by centrifugation at 12,000 x g for 20 min at 4˚C. The protein concentration was determined using a BCA protein content detection kit (cat. no. KGB2101-1000; Nanjing KeyGen Biotech Co., Ltd.), and adjusted to a consistent level. Next, 5X SDS-PAGE protein loading buffer (cat. no. P0286-15 ml; Beyotime Institute of Biotechnology) was added to the protein lysate, which was then heated in a 100˚C water bath for 5 min.

The 10 or 12.5% SDS-PAGE gels were prepared with the Color PAGE Gel Rapid Preparation Kit (cat. no. PG112/PG113; Epizyme; Ipsen Pharma), and a 180 kDa Plus Prestained Protein Marker (cat. no. MP201-01; Vazyme Biotech Co., Ltd.) was used to visualize the protein separation and distribution. A total of 20 μg of protein per lane was transferred from the SDS-PAGE gel to a 0.2-μm PVDF membrane using the wet transfer method, followed by blocking with 5% skim milk solution at room temperature for 2 h. The membranes were then incubated with primary antibody overnight at 4˚C. The following day, after incubation with the secondary antibody for 2 h at room temperature, Pierce™ ECL Western blotting Substrate (cat. no. 32209; Thermo Fisher Scientific, Inc.) was used to visualize the protein bands. The PVDF membrane was washed with TBS-1% Tween-20 (cat. no. T1085; Beijing Solarbio Science & Technology Co., Ltd.) solution between each step at room temperature. The following antibodies were used for western blotting: Rabbit anti-Fn14 antibody (cat. no. bs-2493R; BIOSS), rabbit anti-NF-κB p65 (D14E12) antibody (cat. no. 8242; Cell Signaling Technology, Inc.), rabbit anti-phospho-NFκB p65 (Ser536) antibody (cat. no. 3033; Cell Signaling Technology, Inc.), rabbit anti-NLRP3 antibody (cat. no. bs-41293R; BIOSS), mouse anti-RUNX2 antibody (cat. no. ab76956; Abcam), rabbit anti-Sp7/Osterix antibody [EPR21034] (cat. no. ab209484; Abcam), rabbit anti-OPG antibody (cat. no. ab73400; Abcam), mouse anti-ALP antibody [2F4] (cat. no. ab126820; Abcam), rabbit anti-TWEAK antibody (cat. no. PK93318; Abmart Pharmaceutical Technology Co., Ltd.), mouse anti-β-actin antibody (cat. no. T200068-8F10; ZENBIO Biotechnology Co., Ltd.), goat anti-mouse IgG H&L (HRP) (cat. no. 511103; ZENBIO Biotechnology Co., Ltd.) and goat anti-rabbit IgG H&L (HRP) (cat. no. 511203; ZENBIO Biotechnology Co., Ltd.). All primary antibodies were diluted at a ratio of 1:1,000, and all secondary antibodies were diluted at a ratio of 1:5,000. Some of these antibodies were also employed in the immunofluorescence assays. The grayscale values of the bands were semi-quantified using ImageJ 1.8 software (National Institutes of Health).

Establishment of the rat periodontitis model. The animal experiments conducted, including the use of Avertin as an anesthetic, were approved by the Ethics Committee on Animal Welfare and Experimental Animal Care at Zunyi Medical University (approval no. ZMU21-2504-013; Zunyi, China). A total of 20 male Sprague-Dawley rats, aged 6-8 weeks (~250 g), were purchased from Beijing Huafukang Biotechnology Co., Ltd., and randomly assigned to four groups: Blank, PBS, TWEAK and TWEAK-Fn14-IN-1. All animals were housed under specific pathogen-free conditions at the Animal Experiment Center of Zunyi Medical University (Zunyi, China), with a temperature of 22-25˚C, relative humidity of 40-70%, a 12 h light/12 h dark cycle, and free access to food and water, and allowed 1 week of acclimation before the experimental procedures. Periodontitis was induced in the maxillary second molars using the ligature method. No treatment was applied to the Blank group, whereas threads for the PBS group were placed in the periodontal ligature after being soaked in PBS containing 1 μg/ml lipopolysaccharide (LPS) from *Porphyromonas gingivalis* (Pg. LPS; cat. no. tlrl-pglps; InvivoGen). For the TWEAK and TWEAK-Fn14-IN-1 groups, the threads were soaked in 1 μg/ml Pg. LPS solutions containing either 100 ng/ml TWEAK or 15 μM Fn14 inhibitor TWEAK-Fn14-IN-1 (cat. no. HY-113763; MedChemExpress), respectively. After anesthesia with 1.25% Avertin (150 mg/kg; cat. no. B2910-2x10 ml; BMC Life Science Co., Ltd.) administered intraperitoneally, ligatures were placed around the maxillary second molars. The blank control group did not undergo ligature placement. The silk threads were inspected every 3 days, and the medication was replenished accordingly. At the end of the 4-week period, the rats were humanely euthanized by gradually increasing concentrations of CO_2 (30-70% vol/min) in the animal housing cage. Euthanasia was confirmed by the absence of any signs of activity, and cessation of both cardiac and respiratory functions. The maxillae were then harvested for subsequent analysis.

Micro-CT and histological analyses. After fixation with 4% paraformaldehyde at 4˚C for 8 h, the rat maxillae were analyzed for periodontal bone loss using micro-CT. The periodontal furcation area of the maxillary second molars was designated as the region of interest for all groups. Parameters such as the ratio of bone volume to total volume (BV/TV) and the vertical height of periodontal bone loss [measured from the cementoenamel junction (CEJ) to the lowest point of the alveolar bone] were quantified. Following decalcification with an EDTA decalcifying solution (cat. no. E1171; Beijing Solarbio Science & Technology Co., Ltd.), gradient dehydration, clearing and embedding in paraffin, 6-μm-thick sections were prepared. Paraffin sections were deparaffinized in xylene and rehydrated through a graded descending ethanol series before histological and immunofluorescence staining.

Rehydrated sections were subjected to H&E staining using the H&E staining kit (cat. no. G1120; Beijing Solarbio Science & Technology Co., Ltd.). The staining procedure was as follows: Sections were stained with hematoxylin solution for 5 min and differentiated in differentiation solution for 30 sec, followed by eosin staining for 30 sec. Excess stain was gently drained, and the sections were rapidly dehydrated and mounted with neutral resin. The aforementioned procedures were conducted at room temperature.

Masson's trichrome staining was performed using the Masson's Trichrome Staining Kit (cat. no. G1340; Beijing Solarbio Science & Technology Co., Ltd.). Briefly, sections were stained with Weigert's iron hematoxylin solution for 10 min, rinsed with distilled water and differentiated in acidic differentiation solution for 10 sec. Subsequently, sections were stained with Biebrich scarlet-acid fuchsin solution for 5 min, followed by treatment with phosphomolybdic acid solution for 2 min. The sections were then counterstained with aniline blue solution for 2 min, rapidly dehydrated in 95% ethanol for 3 sec, further dehydrated in absolute ethanol for 15 sec, and finally mounted with neutral resin. All procedures were carried out at room temperature.

Tartrate-resistant acid phosphatase (TRAP)/ALP staining was performed using the TRAP/ALP Stain Kit (cat. no. PAH0848; FUJIFILM Wako Pure Chemical Corporation) for osteoclast staining on rat maxillae sections. Briefly, TRAP staining solution was applied to the rehydrated sections, and the slides were incubated at 37˚C in the dark for 30 min. Subsequently, ALP staining solution was applied, and the slides were incubated at 37˚C in the dark for 1 h. Afterwards, the sections were counterstained with hematoxylin at room temperature for 5 min, rinsed with deionized water, dried at 37˚C and mounted with neutral resin.

Images of the rat maxilla periodontal tissues stained with H&E, Masson's trichrome and TRAP/ALP were captured using a light microscope. The number of osteoclasts (TRAP-positive, multinucleated cells located in the bone resorption lacunae) in the periodontal tissues at the mesial root of the rat maxillary second molar was quantified using ImageJ 1.8 software (National Institutes of Health).

For immunofluorescence staining of rat maxilla paraffin sections, the tissue sections were dewaxed using xylene at room temperature and then rehydrated with a gradient of decreasing ethanol concentrations at room temperature. The tissue sections were subsequently permeabilized with 0.5% Triton X-100 (cat. no. T8200; Beijing Solarbio Science & Technology Co., Ltd.) at room temperature for 15 min. Antigen retrieval was performed by incubating the sections with 0.4% pepsin (cat. no. CR2304020; Wuhan Servicebio Technology Co., Ltd.) at 37˚C for 30 min, followed by blocking with 5% BSA (cat. no. SW3015; Beijing Solarbio Science & Technology Co., Ltd.) for 1 h at room temperature. The tissue sections were washed with PBS for 5 min at room temperature before and after each step, repeated three times. Rabbit anti-periostin antibody (cat. no. ab14041; Abcam), mouse anti-RUNX2 antibody (cat. no. ab76956; Abcam), mouse anti-CD68 antibody (cat. no. ab201340; Abcam) and rabbit anti-CD163 antibody (cat. no. ab182422; Abcam) were diluted 1:200 and incubated with the sections overnight at 4˚C. The following day, Alexa Fluor 647-conjugated goat anti-rabbit antibody (cat. no. A21244; Invitrogen; Thermo Fisher Scientific, Inc.) and Alexa Fluor 555-conjugated goat anti-mouse antibody (cat. no. A21422; Invitrogen; Thermo Fisher Scientific, Inc.) were diluted 1:400 and incubated with the sections at room temperature for 30 min. DAPI solution (cat. no. C0065; Beijing Solarbio Science & Technology Co., Ltd.) was applied at a 1:5,000 dilution and incubated with the sections at room temperature for 5 min for nuclear staining. Fluorescence images were acquired using the Olympus VS200 Whole Slide Scanning System (fluorescence confocal mode; Olympus Corporation), and the fluorescence intensity was analyzed using ImageJ 1.8 software (National Institutes of Health).

Statistical analysis. All data are presented as the mean ± SD. *In vitro* data were obtained from at least three independent experiments. Significant differences were analyzed using a two-tailed unpaired Student's t-test or one-way ANOVA with Tukey's post hoc test, as appropriate. All statistical analyses and statistical graph generation were performed using GraphPad Prism 9.5 software (Dotmatics). $P<0.05$ was considered to indicate a statistically significant difference.

Results

Identification of PDLSCs. Cell clusters were observed around the primary-cultured human PDL tissue, and after passage to P1, these cells exhibited a spindle-shaped morphology *in vitro* (Fig. 1A), consistent with the characteristics of PDLSCs (25). The PDL-derived cells that expanded to P3 still retained the ability to form colonies (Fig. 1B). The expression profile of surface markers on the cells at P3 was further analyzed using flow cytometry. The cells expressed the mesenchymal surface markers CD44 (100%), CD90 (100%), CD29 (99.6%), CD73 (100%) and CD105 (61.4%), but did not express the endothelial cell markers CD31 (0.2%) and CD34 (0.0%), or the panimmune markers CD45 (0.1%) and CD11b (0.0%) (Fig. 1C). Additionally, these cells underwent osteogenic differentiation (Fig. 1D and E) and exhibited adipogenic differentiation potential (Fig. 1F) when cultured in osteogenic or adipogenic induction medium. In conclusion, the cells isolated from the PDL were identified as PDLSCs.

TWEAK influences the survival, migration and osteogenic differentiation potential of PDLSCs. The ability of PDLSCs to survive and migrate within the periodontal

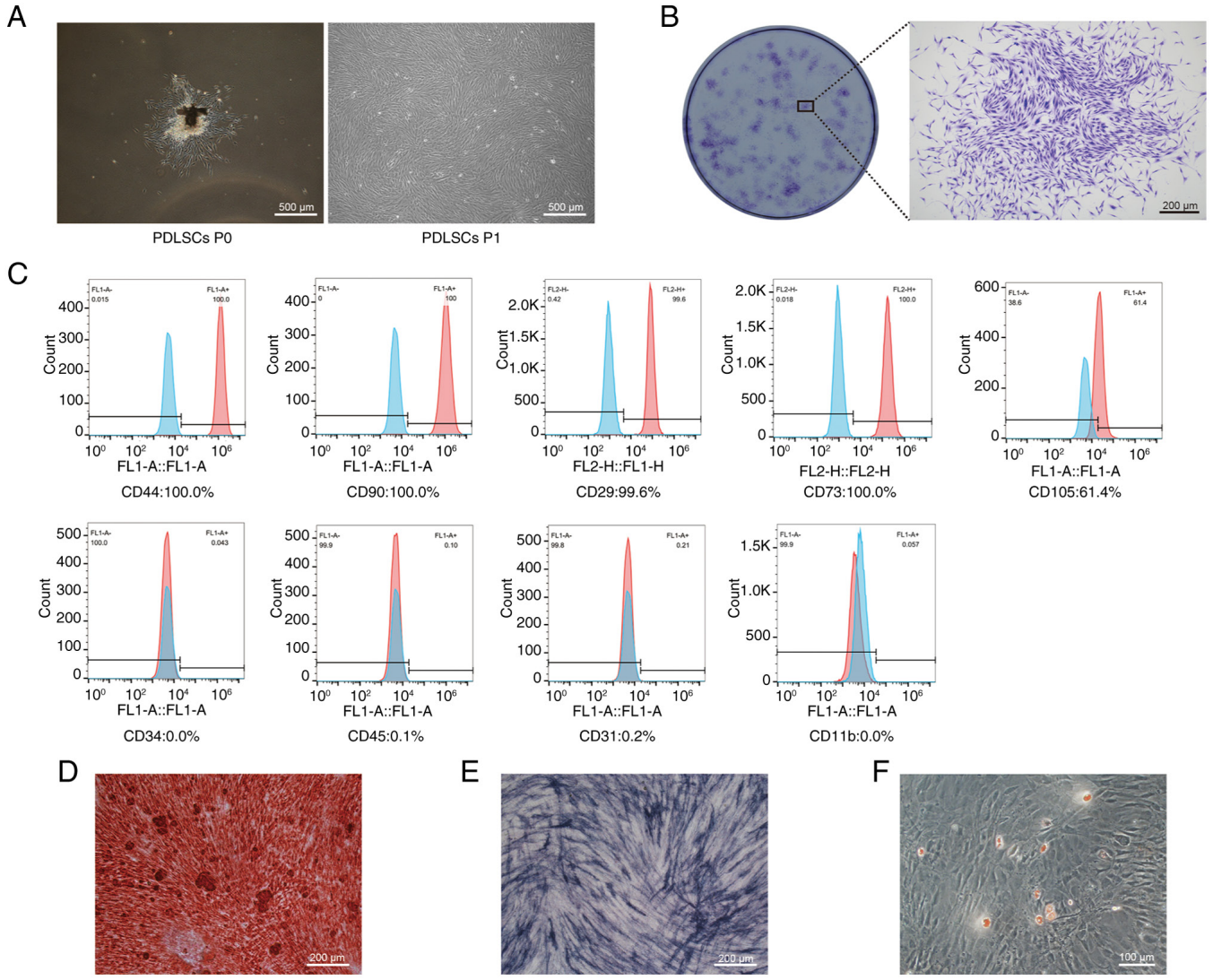

Figure 1. Identification of PDLSCs. (A) Observation of P0 and P1 PDLSCs under a light microscope. Scale bar, 500 μm. (B) PDLSC colonies stained with crystal violet dye. Scale bar, 200 μm. (C) Expression profile of surface markers in PDLSCs quantified using flow cytometry. (D) Mineralized nodules formed by PDLSCs after 14 days of osteogenic induction (stained with Alizarin Red S). Scale bar, 200 μm. (E) Alkaline phosphatase staining of PDLSCs following 7 days of osteogenic induction. Scale bar, 200 μm. (F) Oil red O staining revealed the adipogenic differentiation potential of PDLSCs. Scale bar, 100 μm. P0, primary; P1, first-passage; PDLSC, periodontal ligament stem cell.

injury/inflammatory microenvironment and target specific tissue types for differentiation and regulation is essential for their functional role in tissue repair (26). The present study investigated the effects of exogenous recombinant human TWEAK protein at various concentrations (0, 1, 5, 20, 50 and 100 ng/ml) on the proliferation and apoptosis of PDLSCs. Using the CCK-8 assay, curves showing the effect of 0, 1, 5, 20, 50 and 100 ng/ml TWEAK on the proliferation of PDLSCs were plotted (Fig. 2A). On day 5, the proliferation of PDLSCs was significantly higher in the 1, 5, 20 and 50 ng/ml TWEAK groups compared with the 0 ng/ml TWEAK group (Fig. 2B). However, stimulation with 100 ng/ml TWEAK resulted in a decrease in PDLSC proliferation (Fig. 2A and B). Additionally, induction with 100 ng/ml TWEAK resulted in a high number of TUNEL-positive cells in PDLSCs (Fig. 2C and D), whereas the 0, 1, 5, 20 and 50 ng/ml TWEAK groups exhibited fewer TUNEL-positive cells (Fig. 2D). Based on these findings, we hypothesized that lower concentrations of exogenous TWEAK (≤50 ng/ml) stimulated PDLSC proliferation, potentially reflecting the effect of increased TWEAK expression following early injury or inflammation in MSCs. However, higher concentrations of TWEAK (100 ng/ml) appeared to inhibit PDLSC proliferation and induced apoptosis.

The effect of TWEAK on the migratory behavior of PDLSCs differed from its effect on proliferation. Transwell migration experiments revealed that, compared with PDLSCs without TWEAK treatment, treatment with 1, 5, 20, 50 and 100 ng/ml TWEAK significantly reduced the number of migrating cells (Fig. 3A and B). Furthermore, the inhibitory effect of TWEAK on PDLSC migration became increasingly pronounced at higher concentrations (Fig. 3A and B). The results of the cell scratch wound healing assay further supported the findings from the Transwell migration experiment, indicating that the migration of PDLSCs toward the wound site progressively decreased with increasing TWEAK concentrations (Fig. 3C and D). Thus, it was concluded that TWEAK, regardless of its concentration, disrupted the motility of PDLSCs,

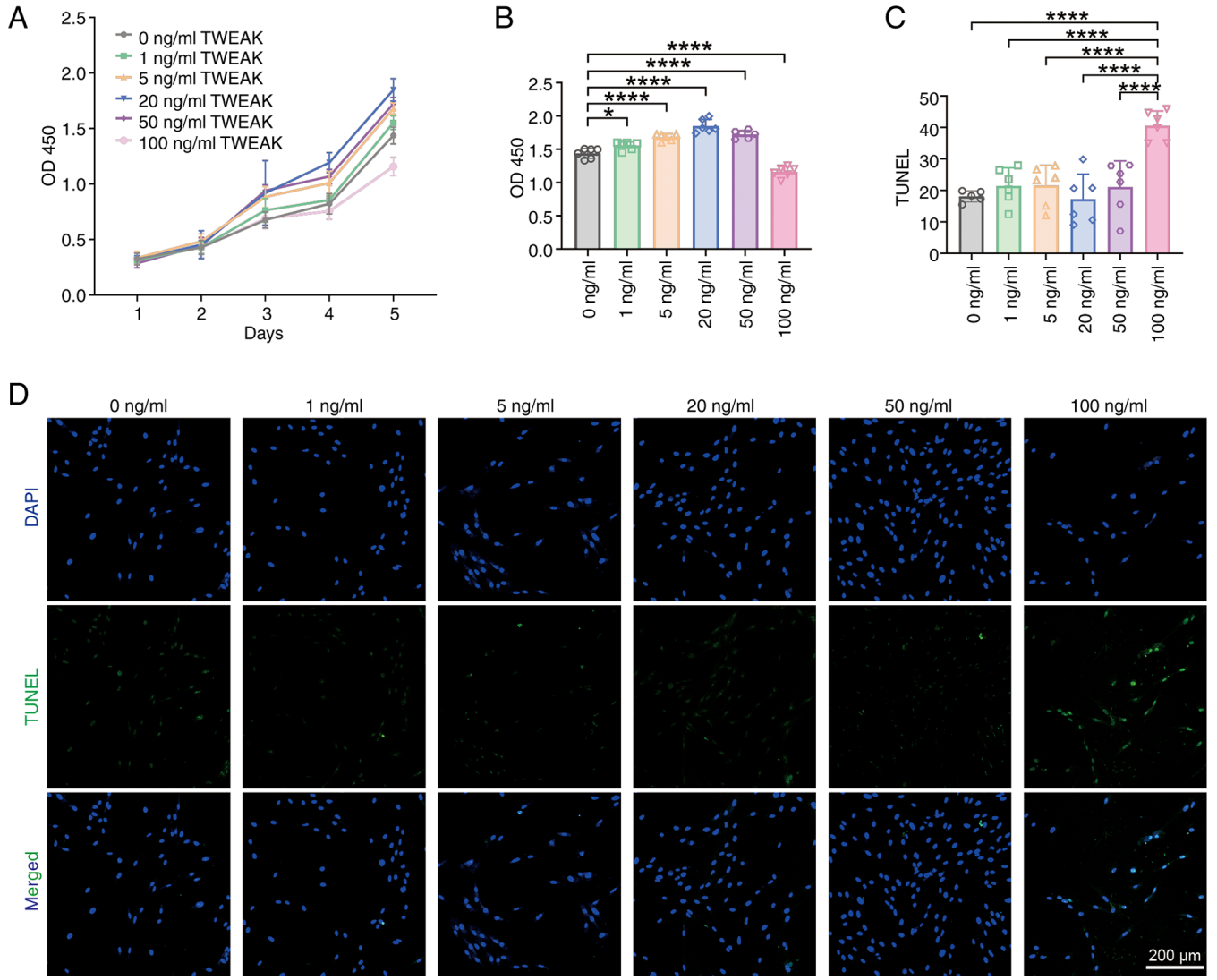

Figure 2. Effects of TWEAK on the proliferation and apoptosis of PDLSCs. (A) Line chart depicting the effects of various concentrations of TWEAK (0, 1, 5, 20, 50 and 100 ng/ml) on PDLSC proliferation over 5 days, as assessed using the CCK-8 assay. (B) Statistical analysis of the CCK-8 data from day 5 of TWEAK stimulation shown in (A). (C) Statistical analysis of the average fluorescence intensity of TUNEL (green) following treatment with varying concentrations of TWEAK (0, 1, 5, 20, 50 and 100 ng/ml). (D) TUNEL assay detecting the effects of various concentrations (0, 1, 5, 20, 50 and 100 ng/ml) of TWEAK on PDLSC apoptosis. Scale bar, 200 μm. Statistical analysis was performed using a one-way ANOVA. *P<0.05; ****P<0.0001. Data are presented as the mean ± SD (n=5 or 6). CCK-8, Cell Counting Kit-8; OD450, optical density at 450 nm; PDLSC, periodontal ligament stem cell; TWEAK, tumor necrosis factor-like weak inducer of apoptosis.

impairing their ability to migrate to sites of periodontal injury or inflammation.

Mineralization is a crucial characteristic of PDLSCs, and contributes to periodontal tissue homeostasis and the regeneration of hard tissues (27). Following stimulation with lower concentrations of TWEAK (5, 20 and 50 ng/ml), both ALP staining (Fig. 3E and F) and the intensity of Alizarin Red staining (Fig. 3G and H) increased with increasing TWEAK concentrations. However, at a concentration of 100 ng/ml, both the ALP staining intensity (Fig. 3E and F) and the Alizarin Red staining intensity (Fig. 3G and H) in PDLSCs were significantly reduced. The expression levels of osteogenesis-related genes (*RUNX2*, *SP7*, *ALP* and *OPG*) and proteins (RUNX2, SP7, ALP and OPG) after TWEAK stimulation were further analyzed using RT-qPCR (Fig. 3I) and western blotting (Fig. 3J and K). Consistent with the results of ALP staining (Fig. 3E and F) and Alizarin Red S staining (Fig. 3G and H), 1, 5, 20 and 50 ng/ml TWEAK promoted RUNX2, SP7, ALP and OPG expression at both the mRNA (Fig. 3I) and protein (Fig. 3J and K) levels. These results suggested that lower concentrations (5, 20 and 50 ng/ml) of TWEAK may enhance the mineralization of PDLSCs, thus promoting alveolar bone repair. However, this effect was limited, as the mineralization potential of PDLSCs sharply declined at a TWEAK concentration of 100 ng/ml.

TWEAK induces PDLSCs to regulate the balance of bone metabolism and macrophage polarization in vitro. RANKL and OPG interact with the NF-κB receptor activator to regulate the formation, activation and survival of osteoclasts during bone formation and remodeling under both physiological and pathological conditions (28). Immunofluorescence staining revealed that after TWEAK stimulation at concentrations of 20, 50 and 100 ng/ml, the expression levels of RANKL

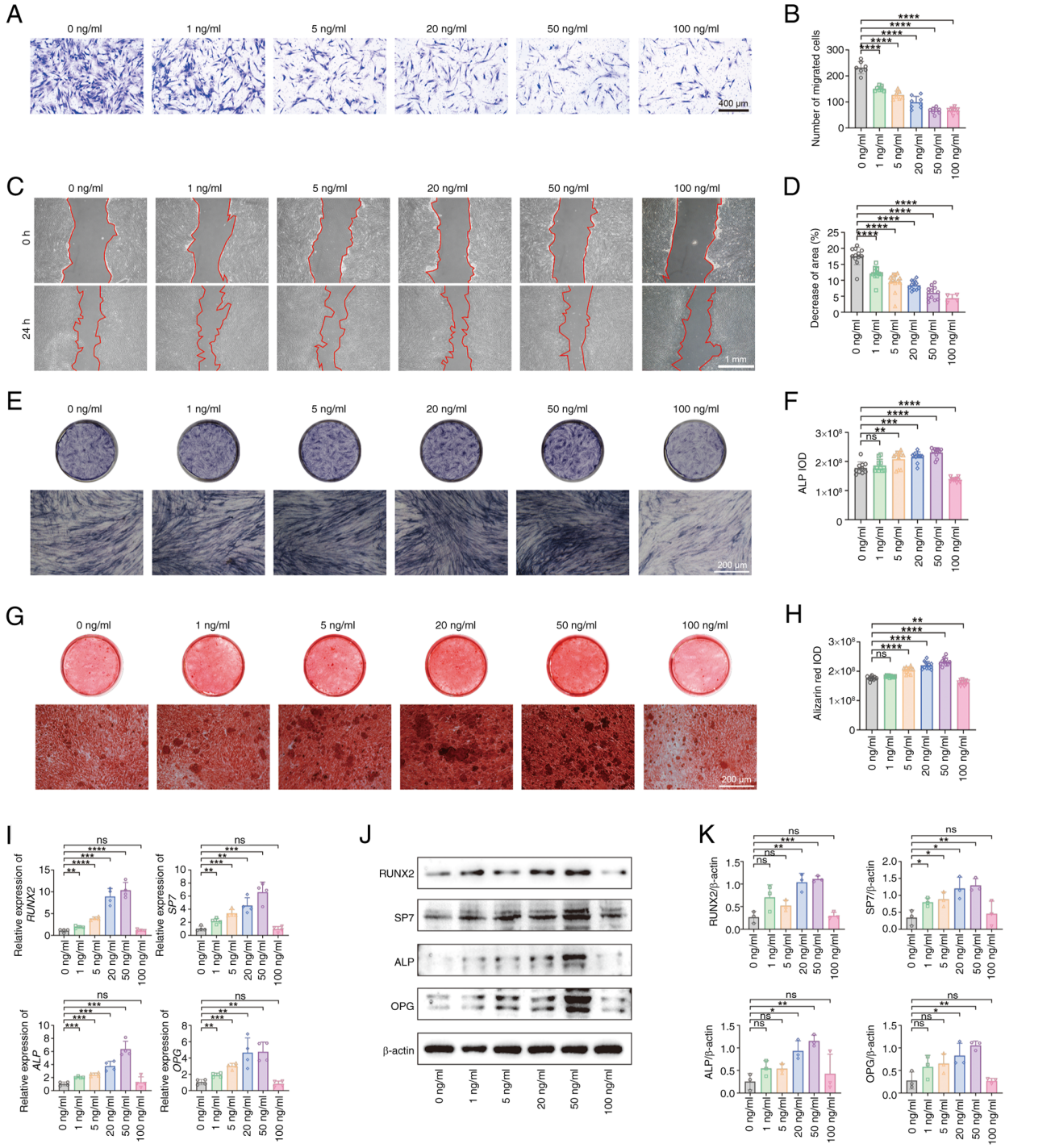

Figure 3. Effects of TWEAK on the migration and osteogenic differentiation of PDLSCs. (A) Effects of various concentrations of TWEAK (0, 1, 5, 20, 50 and 100 ng/ml) on the number of migrating PDLSCs, and (B) quantitative analysis of the number of migrating cells (n=6). Scale bar, 400 μm. (C) Effects of various concentrations of TWEAK on PDLSC migration toward scratch wounds over 24 h, and (D) quantitative analysis of the percentage of wound area reduction (n=12). Scale bar, 1 mm. (E) Effects of various concentrations of TWEAK on ALP staining in PDLSCs, and (F) quantitative analysis of grayscale values from ALP staining (n=6). Scale bar, 200 μm. (G) Alizarin Red staining revealed the effects of various concentrations of TWEAK on PDLSC mineralization, and (H) quantitative analysis of grayscale values from Alizarin Red staining (n=6). Scale bar, 200 μm. (I) Reverse transcription-quantitative PCR was used to assess the mRNA expression levels of *RUNX2*, *SP7*, *ALP* and *OPG* in PDLSCs after TWEAK stimulation (n=4), with *β-actin* serving as the internal control. (J) Western blot analysis of RUNX2, SP7, ALP and OPG protein expression in PDLSCs after TWEAK induction, and (K) semi-quantitative analysis of the gel band intensity, using β-actin as the internal control. Statistical analysis was performed using a one-way ANOVA. *P<0.05; **P<0.01; ***P<0.001; ****P<0.0001. Data are presented as the mean ± SD. ALP, alkaline phosphatase; IOD, integral optical density; ns, not significant; OPG, osteoprotegerin; PDLSC, periodontal ligament stem cell; RUNX2, runt-related transcription factor 2; SP7, Sp7 transcription factor; TWEAK, tumor necrosis factor-like weak inducer of apoptosis.

in PDLSCs were increased significantly (Fig. 4A and B). By contrast, stimulation with 1 or 5 ng/ml TWEAK resulted in a decrease in RANKL expression in PDLSCs (Fig. 4A and B). The expression levels of OPG exhibited a pattern similar to that observed for Alizarin Red staining (Fig. 3G and H), with a gradual increase observed following TWEAK stimulation

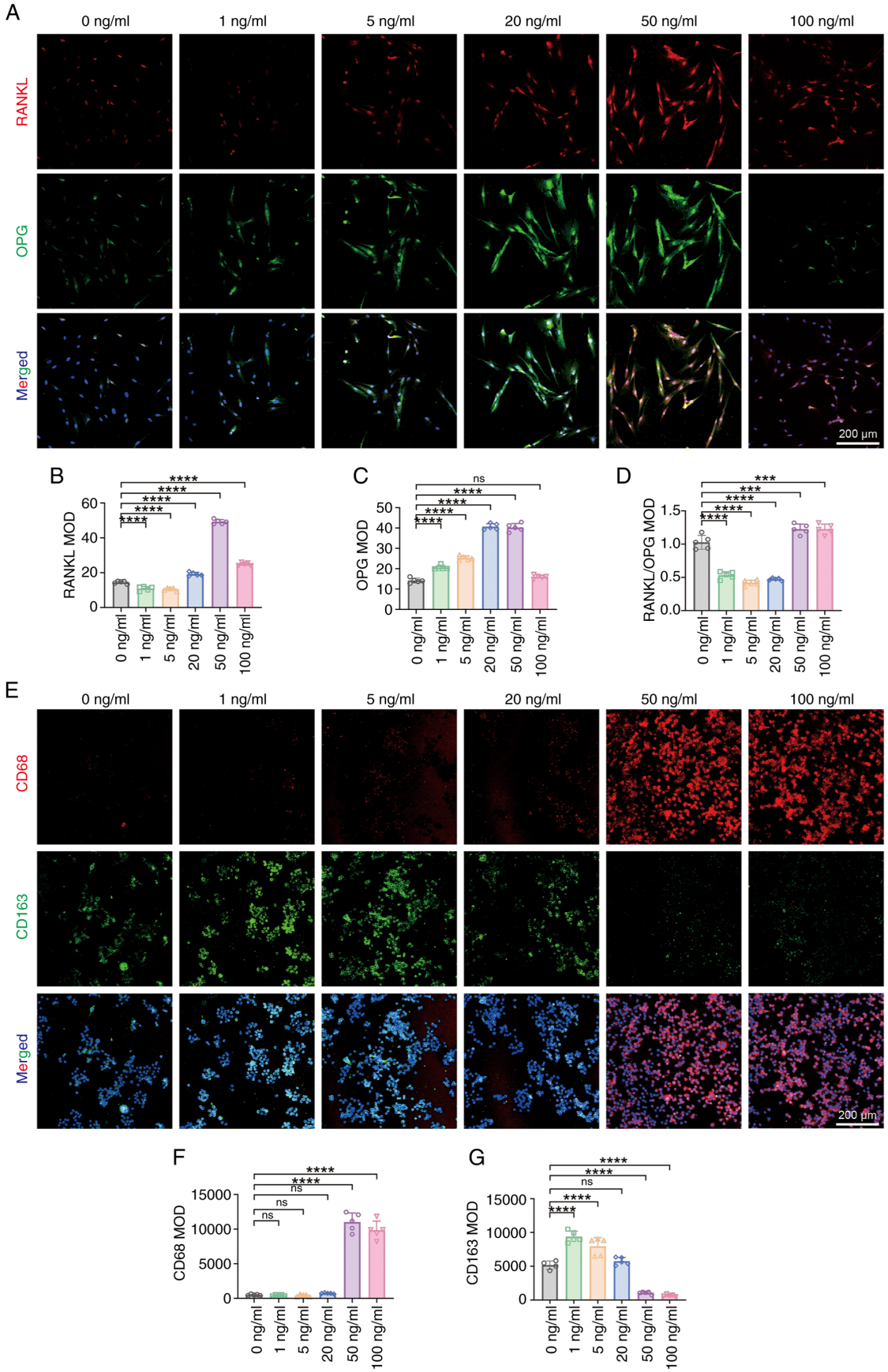

Figure 4. Effects of tumor necrosis factor-like weak inducer of apoptosis on RANKL and OPG expression in PDLSCs and PDLSC-induced macrophage polarization. (A) RANKL (red) and OPG (green) expression in PDLSCs was detected by immunofluorescence staining. Scale bar, 200 μm. Statistical analysis of the MOD values for (B) RANKL and (C) OPG, and (D) their ratio based on (A) (E) CD68 and CD163 expression in RAW264.7 macrophages was assessed by immunofluorescence staining. Scale bar, 200 μm. Statistical analysis of the MOD values for (F) CD68 and (G) CD163 based on (E). Statistical analysis was performed using a one-way ANOVA. ***P<0.001; ****P<0.0001. Data are presented as the mean ± SD (n=5). MOD, mean optical density; ns, not significant; OPG, osteoprotegerin; PDLSC, periodontal ligament stem cell; RANKL, receptor activator of nuclear factor-κB ligand.

at 1, 5 and 20 ng/ml (Fig. 4A and C). By contrast, 100 ng/ml TWEAK did not affect OPG expression compared with that in the 0 ng/ml TWEAK group (Fig. 4A and C). Stimulation with 1, 5 or 20 ng/ml TWEAK reduced the RANKL/OPG ratio in PDLSCs, whereas treatment with 50 or 100 ng/ml TWEAK significantly increased this ratio (Fig. 4D). These results suggested that low concentrations of TWEAK (1, 5 or 20 ng/ml) may inhibit osteoclast formation through the RANKL/OPG system, whereas high concentrations of TWEAK (50 or 100 ng/ml) exert the opposite effect.

The role of MSCs in maintaining microenvironmental homeostasis and promoting tissue regeneration is mediated primarily by their regulation of immune cells (29). The polarization of M2 macrophages is crucial for the stability and regeneration of periodontal tissues, including the cementum and alveolar bone (30,31). PDLSCs were pretreated with various concentrations of TWEAK before being cocultured with macrophages. Immunofluorescence staining was employed to assess the expression levels of CD68 and CD163 in the cells, and the impact of coculturing macrophages with differently pretreated PDLSCs on macrophage polarization was determined. PDLSCs pretreatment with TWEAK at concentrations of 1 or 5 increased the expression of the M2 polarization marker CD163 in macrophages (Fig. 4E and G), whereas the expression of the M1 polarization marker CD68 remained unchanged (Fig. 4E and F). Pretreatment of PDLSCs with TWEAK at concentrations of 50 and 100 ng/ml significantly increased the expression of CD68 in macrophages after co-culture (Fig. 4E and F), while markedly suppressing the expression of CD163 (Fig. 4E and G). These findings (Fig. 4E-G) underscore the concentration-dependent effect of TWEAK on the paracrine secretion of PDLSCs. In summary, we hypothesized that low levels of TWEAK could promote the regulation of periodontal bone metabolism and the immune microenvironment by PDLSCs. Conversely, higher levels of TWEAK disrupted the maintenance of periodontal tissue homeostasis mediated by PDLSCs.

TWEAK induces changes in the PDLSC transcriptome. The present study investigated the underlying mechanism of the effects of TWEAK on the properties of PDLSCs by selecting the 50 and 100 ng/ml TWEAK groups based on the proliferation capacity of PDLSCs (Fig. 2A and B) to examine transcriptome changes in both compensated and decompensated PDLSCs. The Venn diagram indicated that 11,475 genes were co-expressed among the PDLSCs, PDLSCs treated with 50 ng/ml TWEAK and PDLSCs treated with 100 ng/ml TWEAK, with each group exhibiting 118, 108 and 44 uniquely expressed genes, respectively, compared with the other two groups (Fig. 5A). A greater number of differentially expressed genes was identified between the PDLSC group and the PDLSC group treated with 50 ng/ml TWEAK, while the number of differentially expressed genes between the PDLSC group and the PDLSC group treated with 100 ng/ml TWEAK was markedly lower (Fig. 5B). These findings suggested that high concentrations of TWEAK (100 ng/ml) may inhibit PDLSC activity and promote programmed cell death (Fig. 2C and D).

GO analysis revealed that PDLSCs stimulated with 50 ng/ml TWEAK were enriched in biological processes such as 'Response to external stimulus' and 'Cellular response to chemical stimulus' (Fig. 5C), suggesting that 50 ng/ml TWEAK may induce a stress-like state in PDLSCs. The KEGG analysis revealed that, compared with the PDLSCs group, differentially expressed genes in PDLSCs treated with 50 ng/ml TWEAK were significantly enriched in the 'TNF signaling pathway', 'NF-kappa B signaling pathway' and 'NOD-like receptor signaling pathway' (Fig. 5D) (32). Both TWEAK and Fn14 belong to the TNF superfamily, implying that treatment with 50 ng/ml TWEAK may effectively activate TWEAK/Fn14 signaling in PDLSCs. Additionally, the NF-κB pathway is recognized as one of the downstream signaling pathways of the TWEAK/Fn14 axis (33). A study has shown that NF-κB and NLRP3 (34), key components of the NOD-like receptor signaling pathway, are crucial for enhancing the involvement of PDLSCs in periodontitis. Therefore, we hypothesized that TWEAK-Fn14 might regulate the characteristics of PDLSCs through NF-κB and NLRP3.

GO analysis indicated that stimulation of PDLSCs with 100 ng/ml TWEAK was associated with terms such as 'Response to virus', 'Defense response to virus' and 'Innate immune response' (Fig. 5E), and the KEGG analysis results revealed that the 'TNF signaling pathway', 'NF-kappa B signaling pathway' and 'NOD-like receptor signaling pathway' were not among the top 10 enriched pathways (Fig. 5F). We hypothesized that this phenomenon may be attributed to the decompensated state of PDLSCs following 100 ng/ml TWEAK stimulation, as the proliferation of PDLSCs was significantly inhibited, and a substantial number of PDLSCs underwent apoptosis under these conditions (Fig. 2A-D).

The levels of Fn14, NF-κB, phosphorylated NF-κB (P-NF-κB) and NLRP3 in PDLSCs were examined following stimulation with 50 or 100 ng/ml TWEAK to further elucidate whether NF-κB and NLRP3 are downstream signaling pathways of the TWEAK/Fn14 axis. Stimulation with 50 ng/ml TWEAK increased the levels of Fn14, NF-κB, P-NF-κB and NLRP3 (Fig. 5G and H), whereas stimulation with 100 ng/ml TWEAK did not lead to a significant increase in NF-κB or NLRP3 expression (Fig. 5G and H), which was consistent with the sequencing results (Fig. 5F). This phenomenon may be explained by the fact that high-dose TWEAK likely induced an initial upregulation of NF-κB, followed by a decline as cellular integrity was compromised, potentially via apoptosis (Fig. 2D); however, further evidence is required to support this hypothesis. Notably, although there was no statistical significance, P-NF-κB remained slightly elevated at 100 ng/ml (Fig. 5G and H), and the marked suppression of proliferation, migration and osteogenesis, induction of apoptosis, and alterations in the RANKL/OPG ratio (Figs. 2-4) demonstrated PDLSC decompensation under prolonged high TWEAK exposure. Subsequently, lentiviral transfection of PDLSCs with three Fn14-targeting shRNAs demonstrated that shRNA-3 effectively reduced Fn14 expression (Fig. S1A and B), and this was selected for further studies. The direct involvement of Fn14 was further confirmed by experiments showing that silencing of Fn14 in PDLSCs significantly decreased NF-κB, P-NF-κB and NLRP3 levels (Fig. 5I and J). Furthermore, neither stimulation with 50 or 100 ng/ml TWEAK (Fig. 5G and H) nor inhibition of Fn14 expression (Fig. 5I and J) altered the P-NF-κB/NF-κB ratio, indicating that TWEAK/Fn14 did not

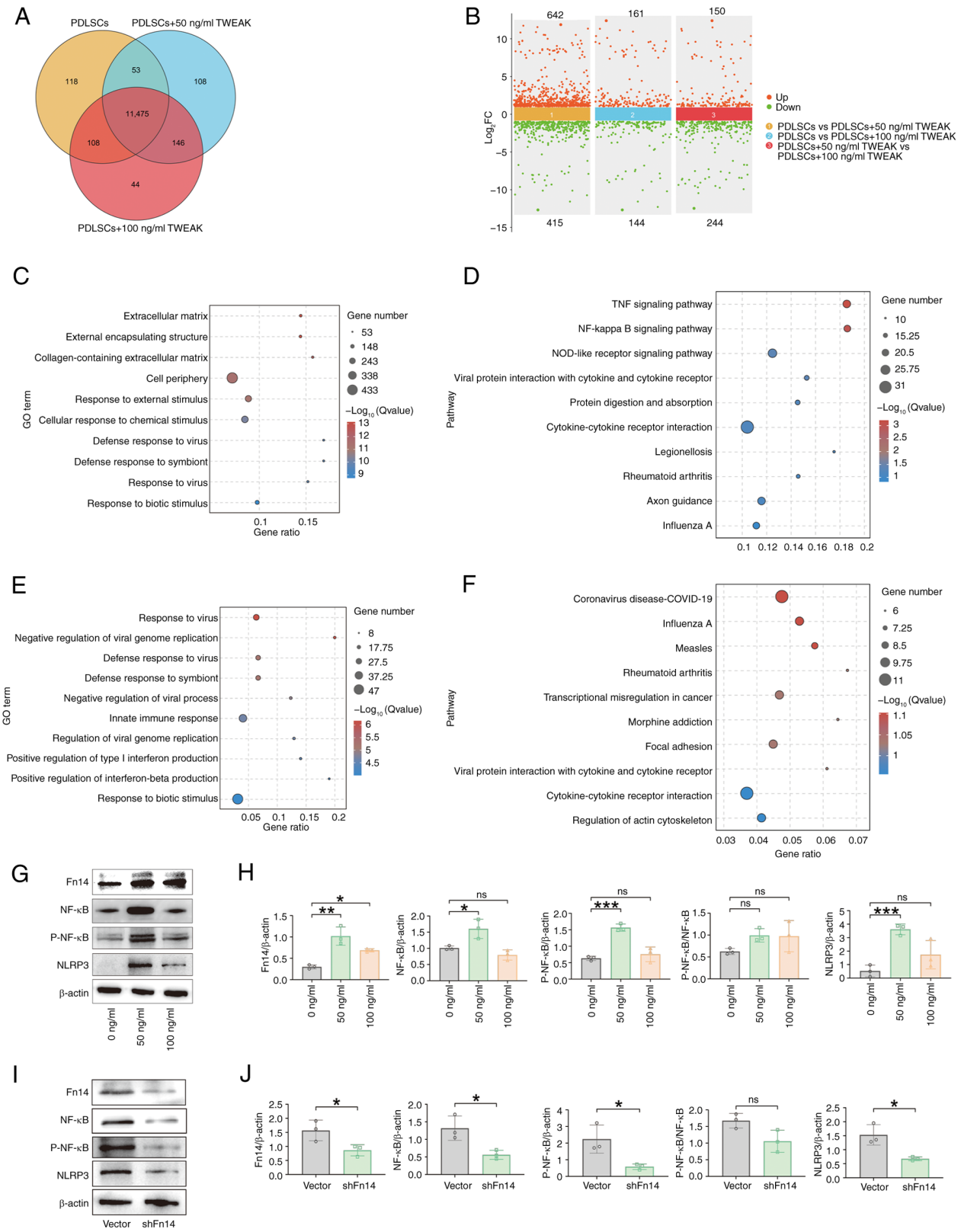

Figure 5. Transcriptome analysis of the effect of TWEAK treatment on PDLSCs. (A) Venn diagram illustrating differentially expressed genes in PDLSCs following TWEAK treatment. (B) Multipoint differential scatter plot showing differentially expressed genes in PDLSCs following TWEAK treatment. (C) GO enrichment analysis comparing PDLSCs and PDLSCs treated with 50 ng/ml TWEAK. (D) KEGG enrichment analysis comparing PDLSCs and PDLSCs treated with 50 ng/ml TWEAK. (E) GO enrichment analysis comparing PDLSCs and PDLSCs treated with 100 ng/ml TWEAK. (F) KEGG enrichment analysis comparing PDLSCs and PDLSCs treated with 100 ng/ml TWEAK. (G) Western blot analysis was conducted to detect the levels of Fn14, NF-κB, P-NF-κB and NLRP3 in PDLSCs stimulated with 50 and 100 ng/ml TWEAK. (H) Statistical analysis of protein band intensities from (G) (n=3). (I) Western blot analysis of the levels of Fn14, NF-κB, P-NF-κB and NLRP3 in PDLSCs after Fn14 was silenced using an shRNA. (J) Statistical analysis of protein band intensities from (I) (n=3). Statistical analysis was performed using (G and H) one-way ANOVA or (I and J) a two-tailed Student's t-test. *P<0.05; **P<0.01; ***P<0.001. Data are presented as the mean ± SD. FC, fold change; Fn14, fibroblast growth factor-inducible 14; GO, Gene Ontology; KEGG, Kyoto Encyclopedia of Genes and Genomes; NLRP3, NOD-like receptor thermal protein domain-associated protein 3; ns, not significant; P-, phosphorylated; PDLSC, periodontal ligament stem cell; shRNA/sh, short hairpin RNA; TWEAK, tumor necrosis factor-like weak inducer of apoptosis.

significantly affect NF-κB activation in PDLSCs. Overall, these results suggested that the TWEAK/Fn14 signaling axis could increase the levels of NF-κB, P-NF-κB and NLRP3 in PDLSCs, thereby influencing their biological functions.

Inhibition of Fn14 and NF-κB effectively attenuates TWEAK-induced changes in PDLSC characteristics. The effects of inhibiting the Fn14/NF-κB pathway on TWEAK-induced alterations in PDLSC characteristics were investigated using an shRNA and the NF-κB inhibitor NF-κB-IN-1 to suppress Fn14 and NF-κB expression, respectively. Silencing of Fn14 expression or pretreatment with NF-κB-IN-1 significantly attenuated the stimulatory effect of 50 ng/ml TWEAK on NF-κB, P-NF-κB and NLRP3 levels (Fig. 6A and B). In contrast to NF-κB-IN-1, which decreased the P-NF-κB/NF-κB ratio, Fn14 silencing had no significant effect on this ratio (Fig. 6A and B). Furthermore, inhibition of both Fn14 and NF-κB reversed the stimulatory effect of 50 ng/ml TWEAK on PDLSC proliferation (Fig. 6C and D). ALP staining (Fig. 6E and G) and Alizarin Red staining (Fig. 6F and H) confirmed the results of the proliferation assays, which revealed that the suppression of Fn14 and NF-κB expression reduced the osteogenic differentiation-promoting effects of 50 ng/ml TWEAK on PDLSCs. Additionally, RT-qPCR (Fig. 6I) and western blot (Fig. 6J and K) analyses confirmed that blocking of the Fn14/NF-κB pathway reduced the expression levels of RUNX2, SP7, ALP and OPG in PDLSCs. Furthermore, inhibition of the Fn14/NF-κB pathway prevented the TWEAK-induced increase in the RANKL/OPG ratio in PDLSCs (Fig. 7A-D). Compared with macrophages co-cultured with PDLSCs pretreated with TWEAK, macrophages co-cultured with PDLSCs pretreated with TWEAK after Fn14 and NF-κB inhibition exhibited lower CD68 expression (Fig. 7E and F). Although CD163 expression showed no significant difference (Fig. 7E and G), these results still suggested that inhibition of Fn14 and NF-κB could reverse the TWEAK-induced promotion of M1 polarization in macrophages by PDLSCs (Fig. 7E-G). These results highlighted the crucial role of the Fn14/NF-κB pathway in mediating TWEAK-induced alterations in PDLSC characteristics.

Inhibition of the TWEAK/Fn14/NF-κB/NLRP3 pathway enhances the functional properties of iPDLSCs. iPDLSCs were isolated from inflamed human periodontal tissue to investigate the potential therapeutic effects of targeting the TWEAK/Fn14/NF-κB/NLRP3 pathway in iPDLSCs for the treatment of periodontitis. iPDLSCs were successfully cultured *in vitro*, and the expression of CD44 (99.7%), CD90 (99.5%), CD29 (100%), CD73 (99.7%) and CD105 (26.8%) was maintained through passage 3, while the expression of CD31 (0.13%), CD34 (0.081%), CD45 (0.52%) and CD11b (0.25%) was negligible (Fig. 8A).

Compared with those in PDLSCs derived from healthy tissues, the levels of TWEAK, Fn14, NF-κB, P-NF-κB and NLRP3 in iPDLSCs were increased (Fig. 8B and C), whereas the ratio of P-NF-κB to NF-κB showed no significant difference (Fig. 8B and C). In addition, iPDLSCs exhibited increased apoptosis (Fig. 8D and E), reduced proliferation (Fig. 8F and G), impaired migration (Fig. 8H-K) and diminished osteogenic differentiation potential (Fig. 8L-R) compared with PDLSCs. Subsequently, the efficiency of silencing of Fn14 and NLRP3 in iPDLSCs using shRNAs was validated (Fig. S1C-F). shFn14-3 (Fig. S1C and D) and shNLRP3-1 (Fig. S1E and F) significantly reduced their expression and were thus used in subsequent experiments. Notably, inhibition of Fn14, NF-κB and NLRP3 expression in iPDLSCs led to a significant reduction in apoptosis (Fig. 8D and E), while promoting proliferation (Fig. 8F and G), migration (Fig. 8H-K) and osteogenic differentiation (Fig. 8L-R) compared with those in iPDLSCs.

iPDLSCs exhibited a higher ratio of RANKL/OPG expression (Fig. 9A-D) and a greater ability to promote the M1 polarization of macrophages (Fig. 9E-G) compared with PDLSCs. After inhibiting the expression of Fn14, NF-κB or NLRP3, the expression of RANKL in iPDLSCs was downregulated (Fig. 9A and B), the expression of OPG was upregulated (Fig. 9A and C) and the ratio of RANKL/OPG expression was decreased (Fig. 9A and D). In addition, when iPDLSCs with inhibited expression of Fn14, NF-κB and NLRP3 were cocultured with macrophages, their ability to promote the M1 polarization of macrophages was inhibited (Fig. 9E-G). These results indicated that targeting of the TWEAK/Fn14/NF-κB/NLRP3 pathway in iPDLSCs is a potential strategy for the treatment of periodontitis.

Fn14 inhibition alleviates periodontitis in rats. A rat periodontitis model was treated with recombinant TWEAK protein and the Fn14 inhibitor TWEAK-Fn14-IN-1 to further evaluate the potential role of the TWEAK/Fn14 pathway in the progression and treatment of periodontitis. Micro-CT analysis revealed that, compared with healthy rats (control group), periodontitis rats (PBS group) exhibited marked alveolar bone resorption around the second molars (Fig. 10A), an increased distance from the alveolar bone crest (ABC) to the CEJ (Fig. 10B) and a marked decrease in the BV/TV at the furcation area (Fig. 10C). Furthermore, TWEAK exacerbated alveolar bone loss in periodontitis rats (Fig. 10A), increased the ABC-CEJ distance (Fig. 10B) and decreased the BV/TV (Fig. 10C). Treatment with TWEAK-Fn14-IN-1 effectively reduced alveolar bone loss in periodontitis model rats (Fig. 10A), decreased the ABC-CEJ distance (Fig. 10B) and partially restored the BV/TV (Fig. 10C).

The histopathological examination further validated the successful establishment of the rat periodontitis model (Fig. 10D-M). In contrast to that in healthy periodontal tissues, the epithelial barrier in periodontitis samples was disrupted (Fig. 10D), with a disordered fiber alignment and collagen loss in the PDL (Fig. 10E). Additionally, although not statistically significant, there was a trend toward an increased number of osteoclasts in the PDL (Fig. 10F and G). Immunofluorescence staining further revealed an increase in the number of $CD68^+$ macrophages within periodontitis tissues (Fig. 10H and K), accompanied by significant downregulation of the homeostasis-related proteins RUNX2 and periostin (Fig. 10I, L and M). The exogenous recombinant TWEAK protein further exacerbated damage to the epithelial barrier of periodontal tissues, with extensive immune cell infiltration observed beneath the epithelium (Fig. 10D). Immunofluorescence staining confirmed that these infiltrating cells were $CD68^+$ macrophages (Fig. 10H, J and K). The

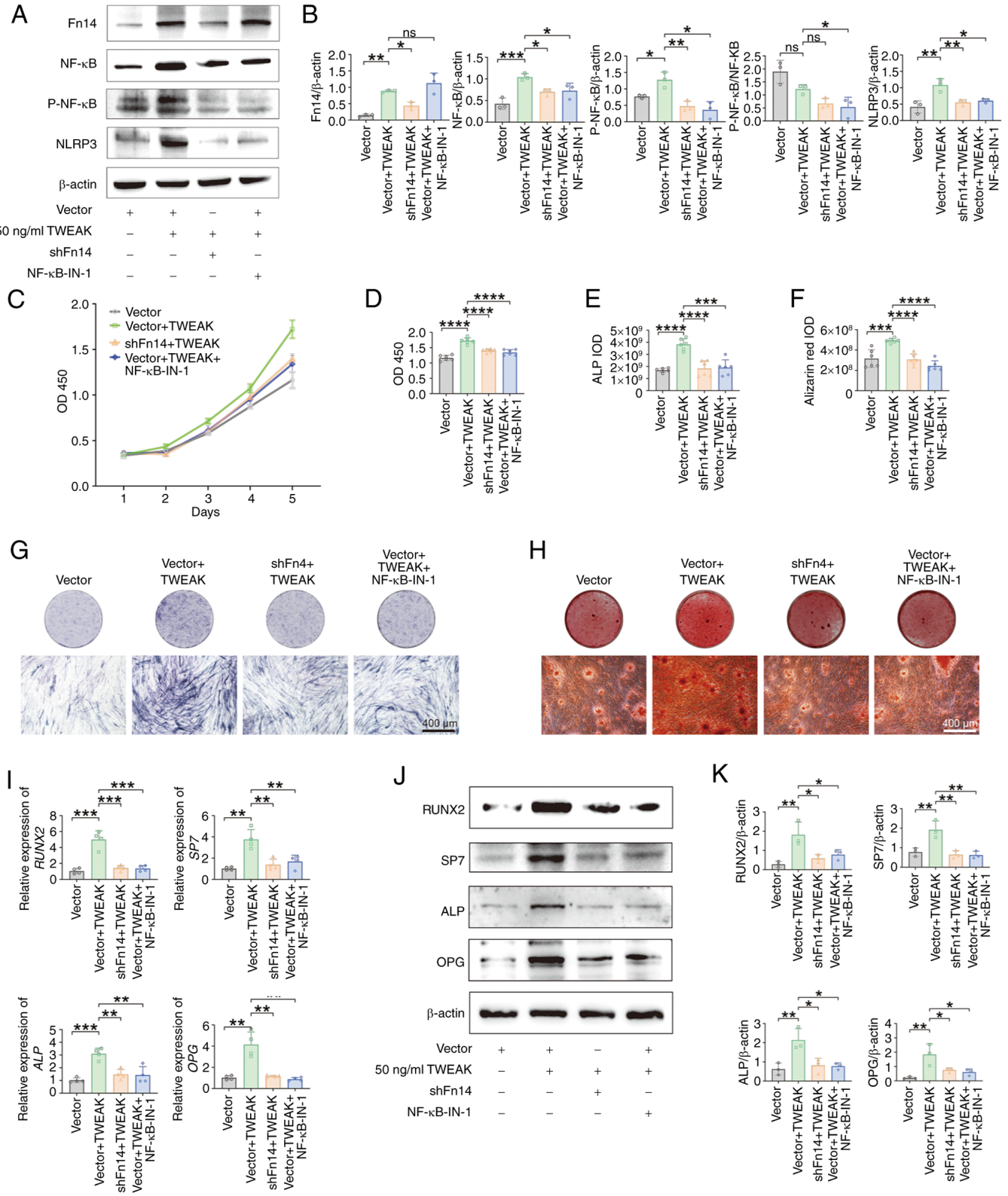

Figure 6. Inhibition of Fn14 and NF-κB effectively blocks TWEAK-induced alterations in PDLSC characteristics. (A) Western blot analysis was conducted to assess the levels of Fn14, NF-κB, P-NF-κB and NLRP3 in PDLSCs. (B) Statistical analysis of the intensities of the protein bands shown in (A) (n=3). (C) A CCK-8 assay was performed to generate the proliferation curve of PDLSCs. (D) Statistical analysis of the OD450 values of cells from each group on day 5 of the CCK-8 assay, as presented in (C) (n=6). (G) Results of ALP staining and (E) the corresponding statistical analysis of PDLSCs after osteogenic induction (n=6). Scale bar, 400 μm. (H) Results of Alizarin Red staining and (F) the corresponding statistical analysis of PDLSCs following osteogenic induction (n=6). Scale bar, 400 μm. (I) Reverse transcription-quantitative PCR was used to assess the mRNA expression levels of *RUNX2*, *SP7*, *ALP* and *OPG* in PDLSCs, with *β-actin* serving as an internal reference (n=4). (J) Western blot analysis was performed to detect the protein expression levels of RUNX2, SP7, ALP and OPG in PDLSCs, and (K) the grayscale values of the gel images were semi-quantitatively analyzed, with β-actin used as an internal reference (n=3). Statistical analysis was performed using a one-way ANOVA. *P<0.05; **P<0.01; ***P<0.001; ****P<0.0001. Data are presented as the mean ± SD. ALP, alkaline phosphatase; CCK-8, Cell Counting Kit-8; Fn14, fibroblast growth factor-inducible 14; IOD, integral optical density; NLRP3, NOD-like receptor thermal protein domain-associated protein 3; ns, not significant; OD450, optical density at 450 nm; OPG, osteoprotegerin; P-, phosphorylated; PDLSC, periodontal ligament stem cell; RUNX2, runt-related transcription factor 2; sh, short hairpin RNA; SP7, Sp7 transcription factor; TWEAK, tumor necrosis factor-like weak inducer of apoptosis.

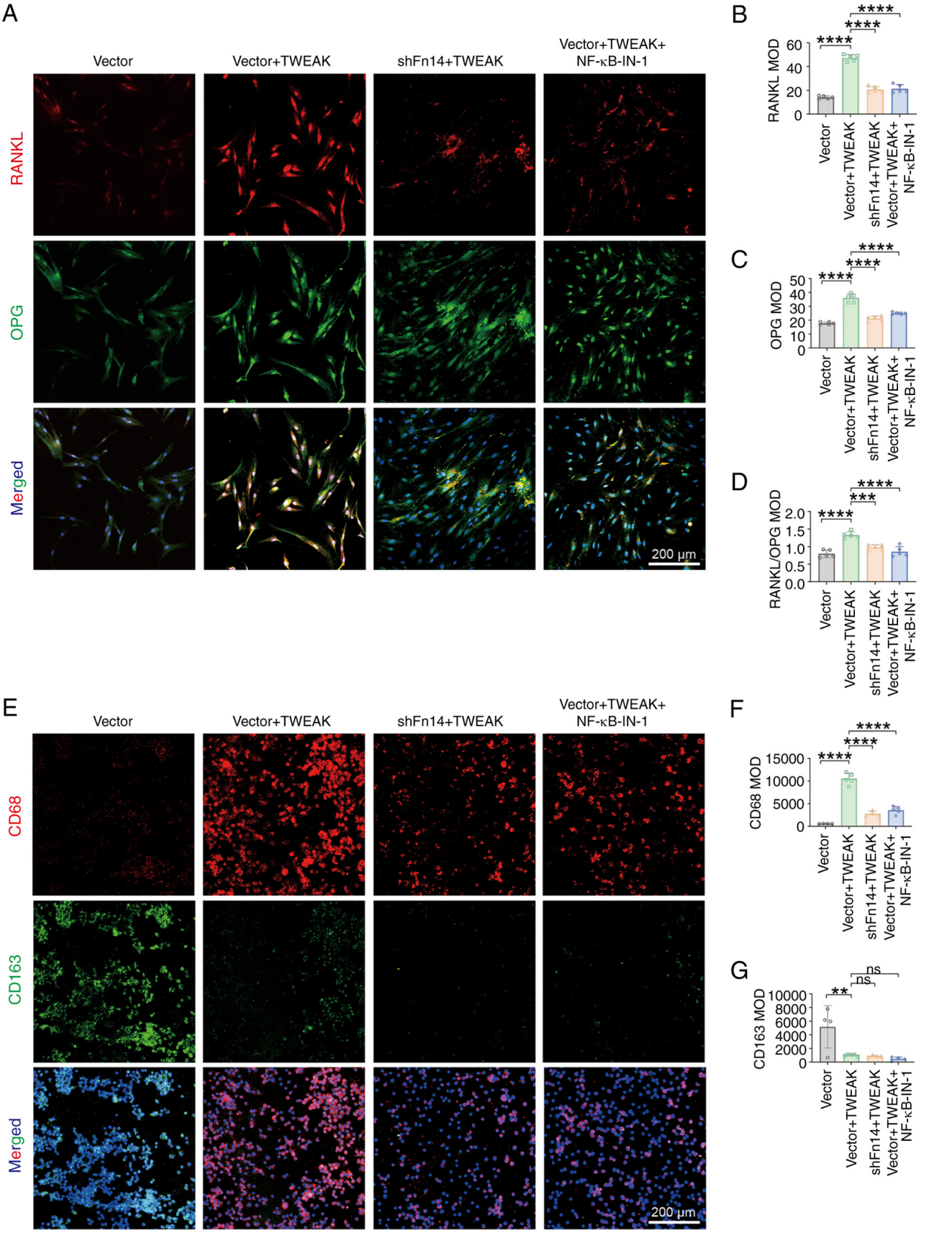

Figure 7. Inhibition of Fn14 and NF-κB effectively blocks TWEAK-induced alterations in the microenvironmental regulatory potential of PDLSCs. (A) Expression levels of OPG (green) and RANKL (red) in PDLSCs were detected by immunofluorescence staining, followed by quantitative analysis of the MOD values for (B) RANKL and (C) OPG, and (D) the MOD ratio of RANKL/OPG (n=5). Scale bar, 200 μm. (E) Expression levels of CD68 and CD163 in RAW264.7 macrophages were detected by immunofluorescence staining, followed by quantitative analysis of the MOD values for (F) CD68 and (G) CD163 (n=5). Scale bar, 200 μm. Statistical analysis was performed using a one-way ANOVA. **P<0.01; ***P<0.001; ****P<0.0001. Data are presented as the mean ± SD. Fn14, fibroblast growth factor-inducible 14; MOD, mean optical density; ns, not significant; OPGa, osteoprotegerin; PDLSC, periodontal ligament stem cell; RANKL, receptor activator of nuclear factor-κB ligand; sh, short hairpin RNA; TWEAK, tumor necrosis factor-like weak inducer of apoptosis.

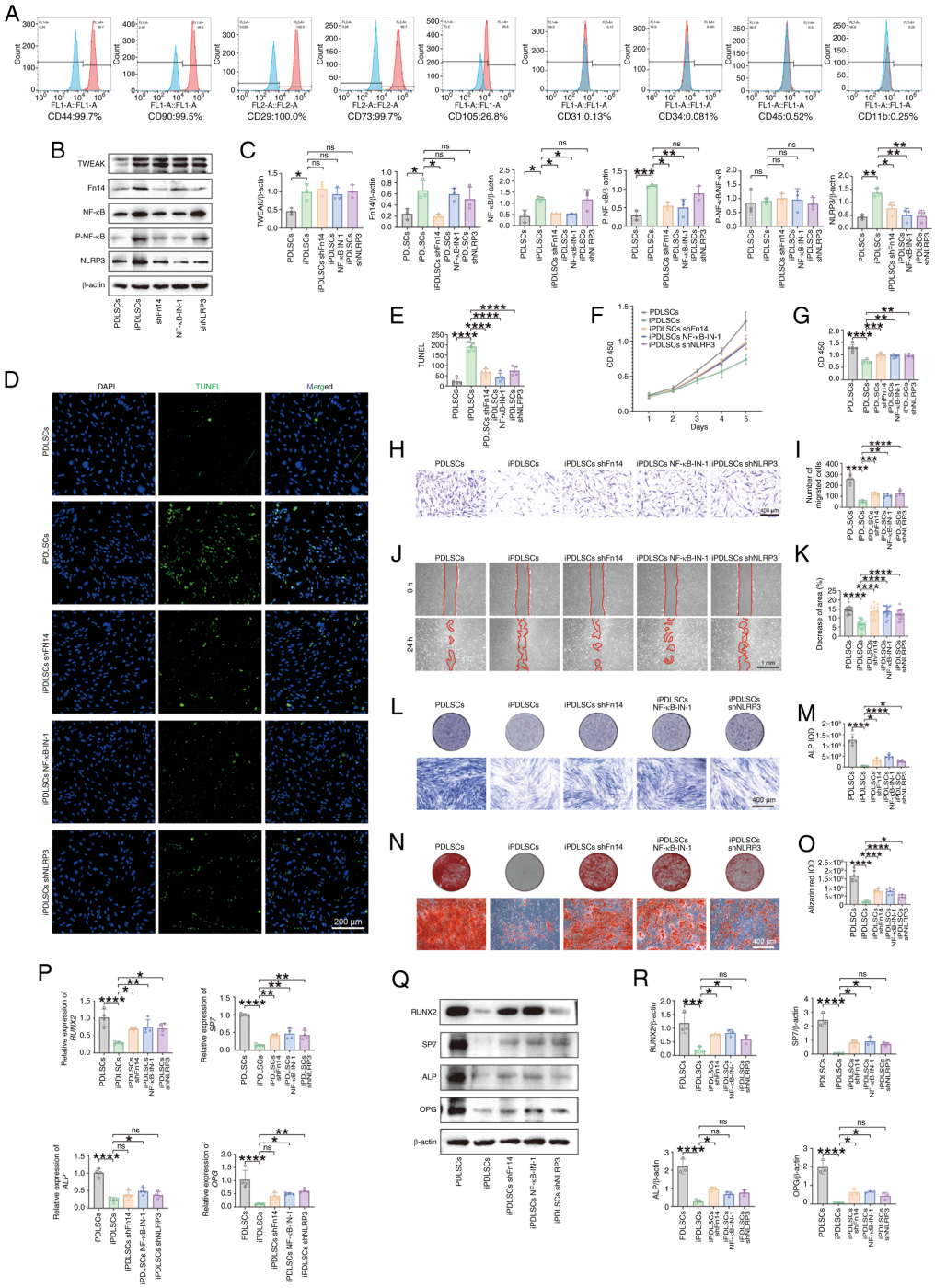

Figure 8. Inhibition of the TWEAK/Fn14/NF-κB/NLRP3 pathway enhances the functional properties of iPDLSCs. (A) Expression profile of surface markers in iPDLSCs quantified using flow cytometry. (B) Levels of TWEAK, Fn14, NF-κB, P-NF-κB and NLRP3 in PDLSCs, iPDLSCs, and iPDLSCs after the downregulation of Fn14, NF-κB and NLRP3, and (C) statistical analysis of the band density values (n=3). (D) Apoptosis levels in PDLSCs, iPDLSCs, and iPDLSCs after downregulation of Fn14, NF-κB and NLRP3 were detected using the TUNEL assay, and (E) statistical analysis of the average fluorescence intensity of TUNEL was performed (n=5). Scale bar, 200 μm. (F) A Cell Counting Kit-8 assay was used to assess the proliferative potential of PDLSCs, iPDLSCs, and iPDLSCs after the downregulation of Fn14, NF-κB and NLRP3, and (G) statistical analysis of the OD450 values on day 5 of the experiment was performed (n=6). (H) Transwell migration assay evaluating the migratory potential of PDLSCs, iPDLSCs, and iPDLSCs after Fn14, NF-κB or NLRP3 downregulation, with (I) quantification of the number of migrated cells (n=6). Scale bar, 400 μm. (J) Wound healing assay evaluating the migratory potential of PDLSCs, iPDLSCs, and iPDLSCs after Fn14, NF-κB or NLRP3 downregulation, with (K) quantification of the percentage of wound closure (%) (n=16). Scale bar, 1 mm. (L) ALP staining was used to evaluate the mineralization potential of PDLSCs, iPDLSCs, and iPDLSCs after downregulation of Fn14, NF-κB or NLRP3, with (M) quantification of the integral optical density of the ALP-stained images (n=6). Scale bar, 400 μm. (N) Alizarin Red staining was used to evaluate the mineralization potential of PDLSCs, iPDLSCs, and iPDLSCs after downregulation of Fn14, NF-κB or NLRP3, with (O) quantification of the integral optical density of the Alizarin Red-stained images (n=6). Scale bar, 400 μm. (P) Reverse transcription-quantitative PCR was used to evaluate the mRNA expression levels of *RUNX2*, *SP7*, *ALP* and *OPG* in PDLSCs, iPDLSCs, and iPDLSCs after the downregulation of Fn14, NF-κB and NLRP3 (n=4). (Q) Western blotting was used to detect the expression levels of RUNX2, SP7, ALP and OPG in PDLSCs, iPDLSCs, and iPDLSCs after the downregulation of Fn14, NF-κB and NLRP3, and (R) statistical analysis of the band density values was performed (n=3). Statistical analysis was performed using a one-way ANOVA. *P<0.05; **P<0.01; ***P<0.001; ****P<0.0001. Data are presented as the mean ± SD. ALP, alkaline phosphatase; Fn14, fibroblast growth factor-inducible 14; IOD, integral optical density; iPDLSC, inflammatory PDLSC; NLRP3, NOD-like receptor thermal protein domain-associated protein 3; ns, not significant; OD450, optical density at 450 nm; OPG, osteoprotegerin; P-, phosphorylated; PDLSC, periodontal ligament stem cell; RUNX2, runt-related transcription factor 2; sh, short hairpin RNA; SP7, Sp7 transcription factor; TWEAK, tumor necrosis factor-like weak inducer of apoptosis.

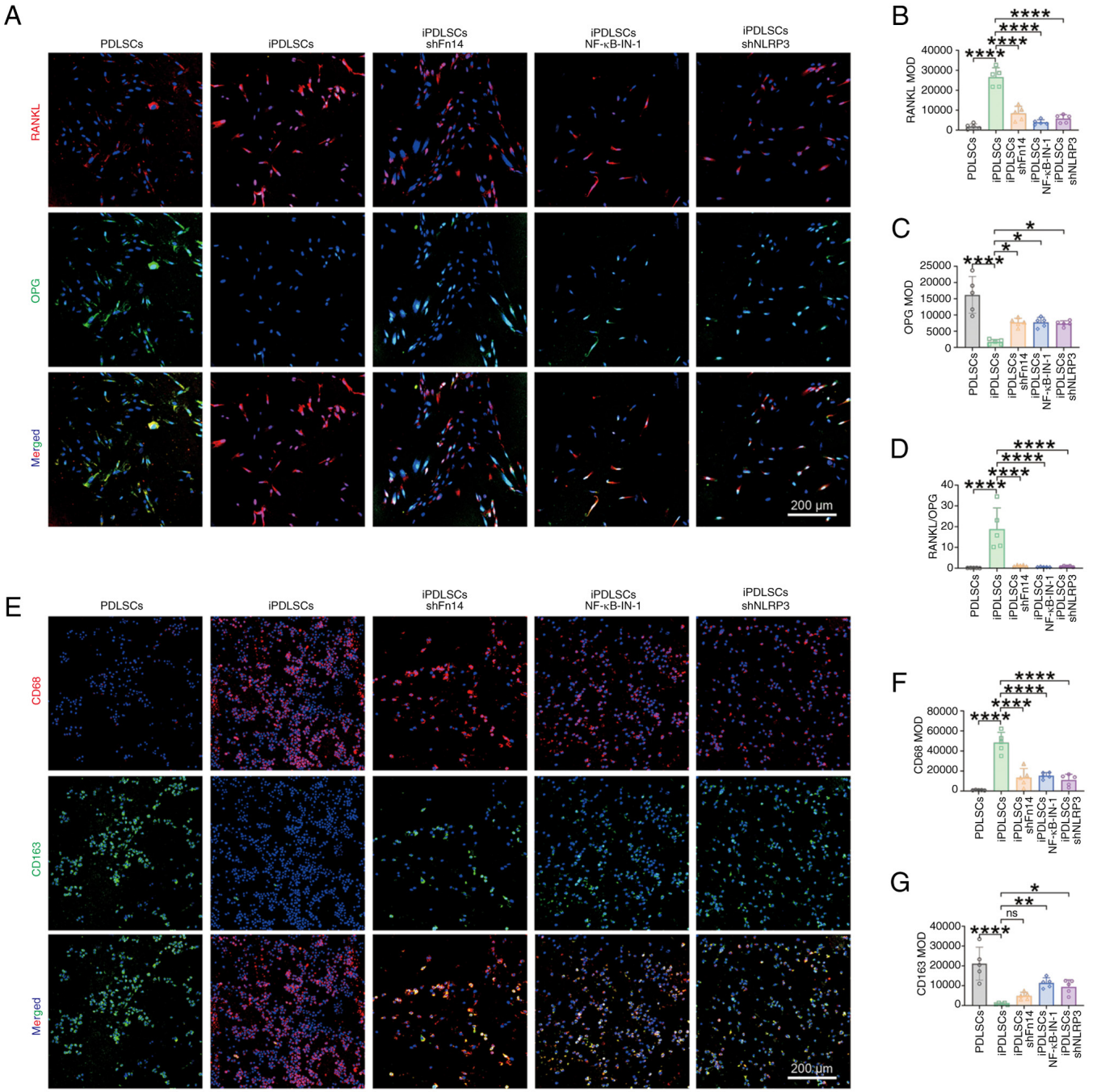

Figure 9. Effect of inhibition of the tumor necrosis factor-like weak inducer of apoptosis/Fn14/NF-κB/NLRP3 pathway on the microenvironmental regulatory ability of iPDLSCs. (A) Immunofluorescence staining was used to detect the expression levels of RANKL and OPG in PDLSCs, iPDLSCs, and iPDLSCs after the downregulation of Fn14, NF-κB and NLRP3, followed by statistical analysis of the average optical density values of (B) RANKL and (C) OPG, and (D) the RANKL/OPG ratio (n=5). Scale bar, 200 μm. (E) Immunofluorescence staining was used to detect the expression levels of CD68 and CD163 in macrophages cocultured with PDLSCs, iPDLSCs, and iPDLSCs after the downregulation of Fn14, NF-κB and NLRP3, followed by statistical analysis of the average optical density values of (F) CD68 and (G) CD163 (n=5). Scale bar, 200 μm. Statistical analysis was performed using a one-way ANOVA. *P<0.05; **P<0.01; ****P<0.0001. Data are presented as the mean ± SD. Fn14, fibroblast growth factor-inducible 14; iPDLSC, inflammatory PDLSC; MOD, mean optical density; NLRP3, NOD-like receptor thermal protein domain-associated protein 3; ns, not significant; OPG, osteoprotegerin; PDLSC, periodontal ligament stem cell; RANKL, receptor activator of nuclear factor-κB ligand; sh, short hairpin RNA.

integrity of the PDL structure was severely compromised (Fig. 10D and E), and the number of osteoclasts in periodontal tissues was significantly increased (Fig. 10F and G). By contrast, treatment with TWEAK-Fn14-IN-1 protected the epithelial barrier of periodontal tissues (Fig. 10D), preserved the collagen fibers beneath the epithelium (Fig. 10E) and tended to maintain the mineralized tissue components (Fig. 10G) compared with the PBS group. Furthermore, TWEAK-Fn14-IN-1 reduced the distribution of CD68^{+} macrophages (Fig. 10H, J and K) in periodontal tissues and preserved the expression of RUNX2 and periostin in periodontal tissues (Fig. 10I, L and M) compared with the PBS group.

Taken together, these results suggested that TWEAK treatment significantly promoted the progression of periodontal

inflammation and tissue destruction, whereas targeting of Fn14 alleviated the progression of periodontitis and protected periodontal tissue homeostasis.

Discussion

The TWEAK/Fn14 pathway is recognized as an immune switch that regulates tissue responses (6). TWEAK/Fn14 expression is upregulated in response to acute stimulation, and serves a role in tissue regeneration and repair (6). Previous studies have shown increased expression of TWEAK in periodontal tissues or gingival crevicular fluid, suggesting its involvement in the progression of periodontitis (10-12). The present findings revealed that low concentrations of TWEAK enhanced the proliferation, osteogenesis and inhibition of osteoclast formation in PDLSCs, indicating that modest increases in TWEAK levels may promote periodontal homeostasis and counteract the progression of periodontitis. However, higher levels of TWEAK impaired PDLSCs proliferation, migration and osteogenic potential, while promoting their osteoclastogenic differentiation. All TWEAK concentrations (1-100 ng/ml) suppressed PDLSC migration, in contrast to other inflammation-related cytokines, such as IL-17 (35), which promoted PDLSC migration at concentrations of 50 and 100 ng/ml. While the present study demonstrated this inhibition, the precise mechanism underlying TWEAK-induced suppression remains unclear, which is a phenomenon not addressed in the present study. However, elucidating the mechanism of comprehensive inhibition of PDLSC migration by TWEAK is a key issue for future research. This could provide important insights into the altered mechanotransduction capabilities of stem cells in inflammatory microenvironments.

The bidirectional regulatory role of TWEAK extends to the modulation of the periodontal immune microenvironment. Previous studies have emphasized the close relationship between an imbalance in M1/M2 macrophage polarization and periodontal homeostasis, and that M1 macrophages exacerbate the progression of periodontitis (36-38). It has also been confirmed that PDLSCs promote M2 macrophage polarization (19), which is beneficial for maintaining periodontal homeostasis. However, under inflammatory conditions, PDLSCs may undergo a transformation that promotes M1 macrophage polarization, thereby exacerbating periodontitis (39). The present results suggested that the dynamic expression of the TWEAK protein serves a key role in the process by which PDLSCs promote the conversion of macrophages from the M1 phenotype to the M2 phenotype. Critically, iPDLSCs from patients with periodontitis exhibited hyperactivation of the TWEAK/Fn14/P-NF-κB/NLRP3 pathway and an increased M1-polarizing capacity. TWEAK is expressed predominantly by macrophages/monocytes under inflammatory conditions (7,40,41). In the present study, iPDLSCs expressed higher levels of TWEAK and Fn14 than PDLSCs. Additionally, TWEAK has been shown to directly regulate macrophage polarization (42). In periodontal tissues, the TWEAK/Fn14 pathway may therefore serve as a critical mechanism for the interaction between macrophages and PDLSCs, potentially serving a key role in maintaining periodontal homeostasis. Furthermore, the present study demonstrated that TWEAK treatment promoted M1 macrophage infiltration in rat periodontitis tissues, whereas the use of TWEAK-Fn14 inhibitors decreased the number of M1 macrophages present in the periodontitis tissues. These findings suggest that targeting the TWEAK/Fn14 pathway could be a potential strategy for ameliorating immune dysregulation in periodontitis.

PDLSCs serve a pivotal role in maintaining periodontal tissue homeostasis (26). The present study revealed that TWEAK-mediated alterations in PDLSCs characteristics have the potential to remodel the periodontal microenvironment. Notably, the periodontal microenvironment consists of diverse cell populations, including fibroblasts, osteoblasts, osteoclasts, cementoblasts and immune cells. Critically, TWEAK has been shown to modulate these cell types: It suppresses fibroblast activation and promotes regenerative macrophage differentiation in pulmonary fibrosis (43), and simultaneously stimulates osteoblast proliferation while inhibiting the mineralization capacity (44). Therefore, TWEAK likely contributes to periodontal homeostasis and bone remodeling not only by directly targeting PDLSCs but also through the coordinated regulation of these auxiliary cell populations. Further investigations are needed to determine whether TWEAK modulates other cells within the periodontal niche via direct or indirect mechanisms.

At the molecular level, the present study demonstrated that TWEAK modulated the characteristics of PDLSCs via the NF-κB signaling pathway, and similar mechanisms have been observed in other disease models. In ovarian cancer, TWEAK enhances cancer stem cell self-renewal and upregulates the expression of SOX2 via NF-κB pathway activation, thereby promoting tumor recurrence (45). By contrast, during liver regeneration, TWEAK inhibits precursor cell differentiation and promotes malignant transformation through the NF-κB-dependent expression of the DNA-binding protein inhibitor ID-1 (46). Notably, beyond its effects on NF-κB, TWEAK activates multiple signaling cascades involved in disease progression, including promoting osteoclastogenesis in osteoporosis through the MAPK pathway (40), exacerbating inflammatory bone destruction in rheumatoid arthritis via PI3K/Akt activation (47), and regulating hair follicle stem cell proliferation and repair through the modulation of the Wnt/β-catenin signaling pathway (48). This multifaceted interplay suggests that, in periodontitis, the TWEAK/Fn14 axis may cooperate with the MAPK pathway or other signaling cascades in addition to the NF-κB pathway. A key limitation of the present study is the lack of direct experimental assessment of the interactions between the TWEAK/Fn14 axis and non-NF-κB signaling pathways within the periodontal microenvironment. Future studies should aim to quantify these interactions experimentally. Additionally, although key findings were validated using patient-derived iPDLSCs, experiments on macrophages utilized the RAW264.7 cell line rather than primary human periodontal macrophages, which represents a limitation of the present study. Future research is needed to further investigate the *in vivo* regulatory effects of TWEAK/Fn14-mediated changes in PDLSCs on immune cells, including macrophages.

Pathological evidence indicates that alterations in the TNF and NF-κB pathways are associated with changes in

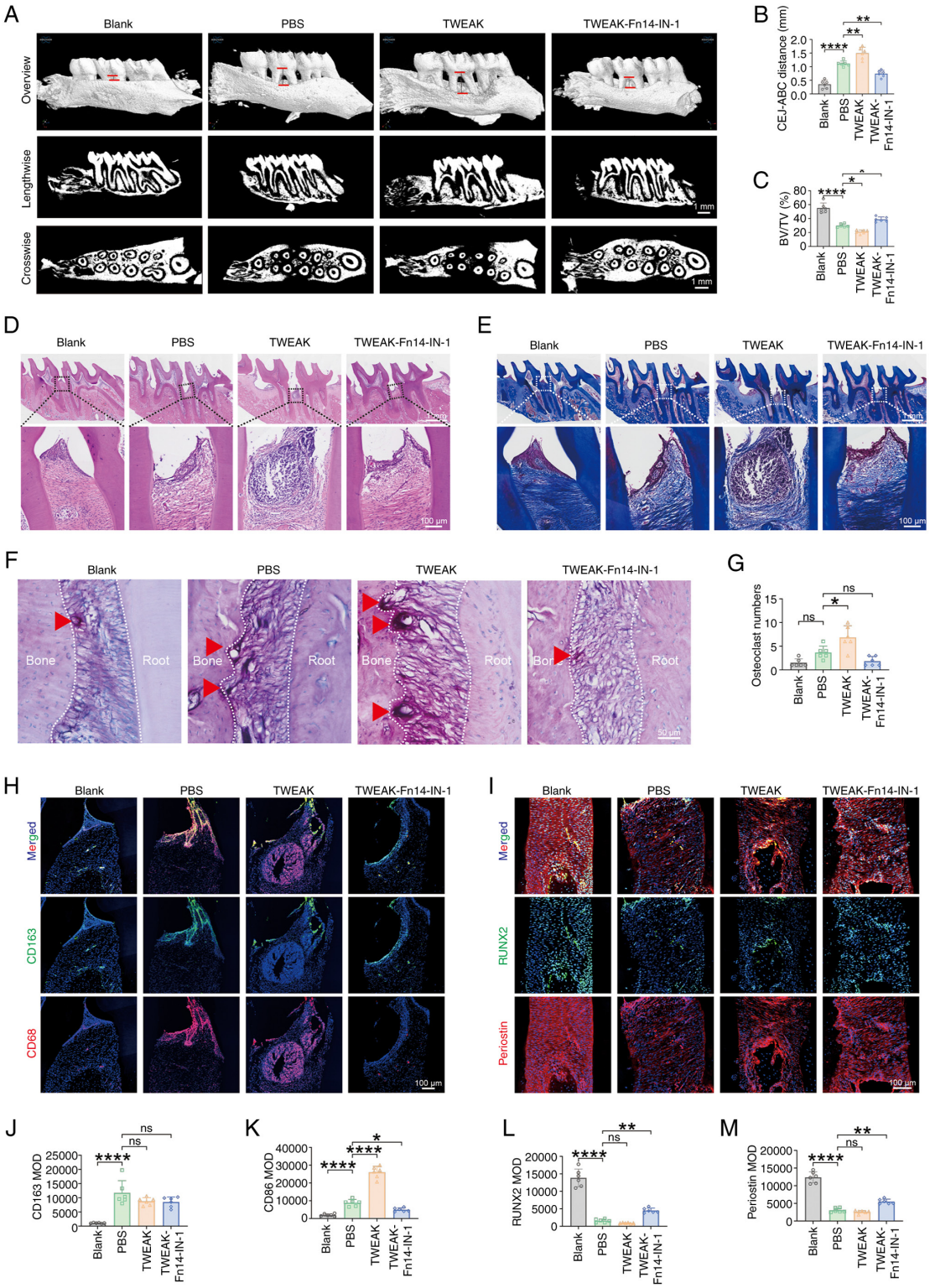

Figure 10. Effects of TWEAK and TWEAK-Fn14-IN-1 on the progression of rat periodontitis. (A) Micro-CT images of the rat maxilla, with the distance between the two red short lines representing the CEJ-ABC distance on the buccal side, and with statistical analysis of the (B) distance of CEJ-ABC (n=6), and (C) BV/TV at the root bifurcation of the maxillary second molar (n=6). Scale bar, 1 mm. Images of (D) H&E and (E) Masson's trichrome staining of rat periodontal tissues. Scale bar, 1 mm (top) or 100 μm (bottom). (F) Representative images of TRAP/alkaline phosphatase double staining in the periodontal tissue of the rat maxillary second molar, with (G) quantification and statistical analysis of osteoclast numbers (TRAP-positive, multinucleated cells located in the bone resorption lacunae) at the mesial root (n=6). Red triangles indicate osteoclasts. Scale bar, 50 μm. (H) Immunofluorescence staining of CD163 (green) and CD68 (red) in periodontal tissues, with (J) quantification of the mean fluorescence intensity of CD163 and (K) quantification of the mean fluorescence intensity of CD68 (n=6). Scale bar, 100 μm. (I) Immunofluorescence staining of RUNX2 (green) and Periostin (red) in periodontal tissues, with (L) quantification of the mean fluorescence intensity of RUNX2 and (M) quantification of the mean fluorescence intensity of Periostin (n=6). Scale bar, 100 μm. Blank represents the unmodeled group, PBS refers to the control group where PBS was used instead of TWEAK or TWEAK-Fn14-IN-1 during modeling, and TWEAK and TWEAK-Fn14-IN-1 represent experimental groups where the recombinant TWEAK protein or TWEAK-Fn14-IN-1 inhibitor was applied, respectively. Statistical analysis was performed using a one-way ANOVA. *P<0.05; **P<0.01; ****P<0.0001. Data are presented as the mean ± SD. ABC, alveolar bone crest; BV/TV, bone volume to total volume; CEJ, cementoenamel junction; Fn14, fibroblast growth factor-inducible 14; MOD, mean optical density; ns, not significant; RUNX2, runt-related transcription factor 2; TRAP, tartrate-resistant acid phosphatase; TWEAK, tumor necrosis factor-like weak inducer of apoptosis.

PDLSC characteristics (49,50). Additionally, Fn14 activation of the NLRP3 inflammasome has been shown to exacerbate acute lung injury (51), whereas NLRP3 dysregulation disrupts the periodontal microenvironment, leading to persistent tissue damage (52). There is also evidence that both *Pseudomonas aeruginosa* (53) and LPS (54) specifically increase NLRP3 expression in PDLSCs, suggesting that PDLSC-mediated regulation of NLRP3 contributes to the disruption of periodontal homeostasis. The present study established the Fn14/NF-κB/NLRP3 axis as the core mechanism through which NF-κB activation drives NLRP3 upregulation, directly mediating high-TWEAK-induced PDLSC dysfunction. This dysfunction is manifested by impaired osteogenic differentiation, enhanced capacity to induce osteoclast formation and increased promotion of M1 macrophage polarization. The present study also revealed that key interventions, including Fn14 inhibitor application, shRNA-mediated Fn14 silencing or pharmacological NF-κB inhibition, effectively blocked NLRP3 hyperactivation, thereby reversing PDLSC dysfunction. This process was achieved by restoring proliferation and migration, increasing osteogenic marker expression, reducing the RANKL/OPG ratio, promoting anti-inflammatory M2 macrophage polarization, and suppressing bone resorption and inflammation. Animal models further confirmed that Fn14 inhibitors significantly alleviated periodontitis-induced bone destruction. Therefore, targeting the Fn14/NF-κB/NLRP3 axis not only repairs dysfunctional PDLSCs but also represents a novel therapeutic approach to reestablish the osteoimmunological balance and treat NLRP3-mediated periodontal pathologies.

Fn14 is expressed at low levels in normal periodontal tissues and lacks a death domain (55), making it a promising therapeutic target for intervention in the progression of advanced periodontitis. Although pharmacological agents targeting the TWEAK/Fn14 axis, including monoclonal antibodies, fusion proteins, immunotoxins and nanoparticle-based formulations, have been explored primarily in oncology research (56-59), their mechanistic principles hold considerable promise for periodontal therapy. Previous studies have shown that anti-TWEAK monoclonal antibodies alleviated chronic inflammation and pathological remodeling (60,61), a strategy for inhibiting TWEAK that may be applicable to periodontitis. The present findings suggest that these strategies not only counteract the pathogenic effects of elevated TWEAK concentrations but also modulate PDLSCs functionality within inflammatory microenvironments to promote tissue regeneration. Building on advancements in cancer therapeutics (56-59), locally deliverable systems can be engineered for intrapocket administration to block the TWEAK/Fn14/NF-κB/NLRP3 pathway in PDLSCs. This approach has the potential to reduce systemic side effects while enhancing regenerative outcomes (62), providing novel strategies to restore periodontal homeostasis. However, clinical implementation still requires further *in vivo* efficacy and safety evaluations.

Acknowledgements

Not applicable.

Funding

The present study was supported by the Guizhou Provincial Department of Education Higher Education Scientific Research Project [Qian Jiao Ji (2022) no. 238], the Science and Technology Fund Project of Guizhou Provincial Health Commission (grant no. gzwkj2024-451), the Guizhou Provincial Health Commission Science and Technology Fund Project (grant no. 2024GZWJKJXM0828), the Zunyi Science and Technology Bureau and Zunyi Medical University Science and Technology Joint Fund [QianShiKeHe HZ Zi (2022) no. 393], the Graduate Research Fund Project of Zunyi Medical University (gran no. ZYK 260), the Zunyi Science and Technology Plan Project [Zunyi Kehe HZ Zi (2022) no. 423], the National Natural Science Foundation of China (grant no. 82060205), and the Guizhou Provincial Health Commission Science and Technology Fund Project (grant no. gzwkj2023-438).

Availability of data and materials

The sequencing data generated in the present study may be found in the National Center for Biotechnology Information Sequence Read Archive under accession number PRJNA1304010 or at the following URL: https://www.ncbi.nlm.nih.gov/sra/PRJNA1304010. The other data generated in the present study may be requested from the corresponding author.

Authors' contributions

CL, XG and LX performed the experimental design. LC, CL, MQ and LX performed the experiments. LC, QL and CL performed the *in silico* bioinformatics analyses. XG, MX, QL and JL contributed intellectual input to experimental design and data analysis. CL, LX and LC wrote the manuscript. CL and LX confirm the authenticity of all the raw data. All authors have read and approved the final version of the manuscript.

Ethics approval and consent to participate

Human periodontal ligament stem cells were derived from extracted teeth collected at the Affiliated Stomatological Hospital of Zunyi Medical University. All human tissue handling protocols were approved by the Ethics Committee of the Affiliated Stomatological Hospital of Zunyi Medical University (approval no. ZYKQ-IRB-CT-2023-065; Zunyi, China), and written informed consent was obtained from all donors. The animal research protocol was approved by the Ethics Committee on Animal Welfare and Experimental Animal Care at Zunyi Medical University (approval no. ZMU21-2504-013; Zunyi, China).

Patient consent for publication

Not applicable.

Competing interests

The authors declare that they have no competing interests.

References

1. Chicheportiche Y, Bourdon PR, Xu H, Hsu YM, Scott H, Hession C, Garcia I and Browning JL: TWEAK, a new secreted ligand in the tumor necrosis factor family that weakly induces apoptosis. J Biol Chem 272: 32401-32410, 1997.
2. Liu Q, Xiao S and Xia Y: TWEAK/Fn14 activation participates in skin inflammation. Mediators Inflamm 2017: 6746870, 2017.
3. Liu J, Liu Y, Peng L, Li J, Wu K, Xia L, Wu J, Wang S, Wang X, Liu Q, *et al*: TWEAK/Fn14 signals mediate burn wound repair. J Invest Dermatol 139: 224-234, 2019.
4. Wang A, Zhang F, Xu H, Xu M, Cao Y, Wang C, Xu Y, Su M, Zhang M and Zhuge Y: TWEAK/Fn14 promotes pro-inflammatory cytokine secretion in hepatic stellate cells via NF-κB/STAT3 pathways. Mol Immunol 87: 67-75, 2017.
5. Johnston AJ and Hoogenraad NJ: Fn14: A new player in cancer-induced cachexia. Curr Opin Clin Nutr Metab Care 19: 316-318, 2016.
6. Burkly LC, Michaelson JS and Zheng TS: TWEAK/Fn14 pathway: An immunological switch for shaping tissue responses. Immunol Rev 244: 99-114, 2011.
7. Ratajczak W, Atkinson SD and Kelly C: The TWEAK/Fn14/CD163 axis-implications for metabolic disease. Rev Endocr Metab Disord 23: 449-462, 2022.
8. Xu WD, Zhao Y and Liu Y: Role of the TWEAK/Fn14 pathway in autoimmune diseases. Immunol Res 64: 44-50, 2016.
9. Wang S, Li L, Cook C, Zhang Y, Xia Y and Liu Y: A potential fate decision landscape of the TWEAK/Fn14 axis on stem and progenitor cells: A systematic review. Stem Cell Res Ther 13: 270, 2022.
10. Yakar N, Guncu GN, Akman AC, Pınar A, Karabulut E and Nohutcu RM: Evaluation of gingival crevicular fluid and peri-implant crevicular fluid levels of sclerostin, TWEAK, RANKL and OPG. Cytokine 113: 433-439, 2019.
11. Kataria NG, Bartold PM, Dharmapatni AA, Atkins GJ, Holding CA and Haynes DR: Expression of tumor necrosis factor-like weak inducer of apoptosis (TWEAK) and its receptor, fibroblast growth factor-inducible 14 protein (Fn14), in healthy tissues and in tissues affected by periodontitis. J Periodontal Res 45: 564-573, 2010.
12. Gur AT, Guncu GN, Akman AC, Pinar A, Karabulut E and Nohutcu RM: Evaluation of GCF IL-17, IL-10, TWEAK, and sclerostin levels after scaling and root planing and adjunctive use of diode laser application in patients with periodontitis. J Periodontol 93: 1161-1172, 2022.
13. Luan X, Zhou X, Trombetta-eSilva J, Francis M, Gaharwar AK, Atsawasuwan P and Diekwisch TGH: MicroRNAs and periodontal homeostasis. J Dent Res 96: 491-500, 2017.
14. Deng DK, Zhang JJ, Gan D, Zou JK, Wu RX, Tian Y, Yin Y, Li X, Chen FM and He XT: Roles of extracellular vesicles in periodontal homeostasis and their therapeutic potential. J Nanobiotechnology 20: 545, 2022.
15. Ravidà A, Qazi M, Rodriguez MV, Galli M, Saleh MHA, Troiano G and Wang HL: The influence of the interaction between staging, grading and extent on tooth loss due to periodontitis. J Clin Periodontol 48: 648-658, 2021.
16. Zhang D, Lin W, Jiang S, Deng P, Liu L, Wang Q, Sheng R, Shu HS, Wang L, Zou W, *et al*: Lepr-Expressing PDLSCs contribute to periodontal homeostasis and respond to mechanical force by piezo1. Adv Sci 10: e2303291, 2023.
17. Zhang Z, Deng M, Hao M and Tang J: Periodontal ligament stem cells in the periodontitis niche: Inseparable interactions and mechanisms. J Leukoc Biol 110: 565-576, 2021.
18. Tomokiyo A, Wada N and Maeda H: Periodontal ligament stem cells: Regenerative potency in periodontium. Stem Cells Dev 28: 974-985, 2019.
19. Liu J, Chen B, Bao J, Zhang Y, Lei L and Yan F: Macrophage polarization in periodontal ligament stem cells enhanced periodontal regeneration. Stem Cell Res Ther 10: 320, 2019.
20. Jin SS, He DQ, Wang Y, Zhang T, Yu HJ, Li ZX, Zhu LS, Zhou YH and Liu Y: Mechanical force modulates periodontal ligament stem cell characteristics during bone remodelling via TRPV4. Cell Prolif 53: e12912, 2020.
21. Zhang Z, Shuai Y, Zhou F, Yin J, Hu J, Guo S, Wang Y and Liu W: PDLSCs regulate angiogenesis of periodontal ligaments via VEGF transferred by exosomes in periodontitis. Int J Med Sci 17: 558-567, 2020.
22. Qiu X, Du Y, Lou B, Zuo Y, Shao W, Huo Y, Huang J, Yu Y, Zhou B, Du J, *et al*: Synthesis and identification of new 4-arylidene curcumin analogues as potential anticancer agents targeting nuclear factor-κB signaling pathway. J Med Chem 53: 8260-73, 2010.
23. Love MI, Huber W and Anders S: Moderated estimation of fold change and dispersion for RNA-seq data with DESeq2. Genome Biol 15: 550, 2014.
24. Livak KJ and Schmittgen TD: Analysis of relative gene expression data using real-time quantitative PCR and the 2(-Delta Delta C(T)) method. Methods 25: 402-408, 2001.
25. Seo BM, Miura M, Gronthos S, Bartold PM, Batouli S, Brahim J, Young M, Robey PG, Wang CY and Shi S: Investigation of multipotent postnatal stem cells from human periodontal ligament. Lancet 364: 149-55, 2004.
26. Zhao X, Lin H, Ding T, Wang Y, Liu N and Shen Y: Overview of the main biological mechanisms linked to changes in periodontal ligament stem cells and the inflammatory microenvironment. J Zhejiang Univ Sci B 24: 373-386, 2023 (In English, Chinese).
27. Jin S, Jiang H, Sun Y, Li F, Xia J, Li Y, Zheng J and Qin Y: Osteogenic differentiation of periodontal membrane stem cells in inflammatory environments. Open Life Sci 17: 1240-1248, 2022.
28. Silva I and Branco JC: Rank/Rankl/opg: Literature review. Acta Reumatol Port 36: 209-218, 2011.
29. Li P, Ou Q, Shi S and Shao C: Immunomodulatory properties of mesenchymal stem cells/dental stem cells and their therapeutic applications. Cell Mol Immunol 20: 558-569, 2023.
30. Nakao Y, Fukuda T, Zhang Q, Sanui T, Shinjo T, Kou X, Chen C, Liu D, Watanabe Y, Hayashi C, *et al*: Exosomes from TNF-α-treated human gingiva-derived MSCs enhance M2 macrophage polarization and inhibit periodontal bone loss. Acta Biomater 122: 306-324, 2021.
31. Huang X, Deng Y, Xiao J, Wang H, Yang Q and Cao Z: Genetically engineered M2-like macrophage-derived exosomes for P. gingivalis-suppressed cementum regeneration: From mechanism to therapy. Bioact Mater 32: 473-487, 2023.
32. Zaitseva O, Hoffmann A, Otto C and Wajant H: Targeting fibroblast growth factor (FGF)-inducible 14 (Fn14) for tumor therapy. Front Pharmacol 13: 935086, 2022.
33. Saitoh T, Nakayama M, Nakano H, Yagita H, Yamamoto N and Yamaoka S: TWEAK induces NF-kappaB2 p100 processing and long lasting NF-kappaB activation. J Biol Chem 278: 36005-36012, 2003.
34. Guo L, Zhang Y, Liu H, Cheng Q, Yang S and Yang D: All-trans retinoic acid inhibits the osteogenesis of periodontal ligament stem cells by promoting IL-1β production via NF-κB signaling. Int Immunopharmacol 108: 108757, 2022.
35. Okić Đorđević I, Kukolj T, Živanović M, Momčilović S, Obradović H, Petrović A, Mojsilović S, Trivanović D and Jauković A: The role of doxycycline and IL-17 in regenerative potential of periodontal ligament stem cells: Implications in periodontitis. Biomolecules 13: 1437, 2023.
36. Zhang B, Yang Y, Yi J, Zhao Z and Ye R: Hyperglycemia modulates M1/M2 macrophage polarization via reactive oxygen species overproduction in Ligature-induced periodontitis. J Periodontal Res 56: 991-1005, 2021.
37. Almubarak A, Tanagala KKK, Papapanou PN, Lalla E and Momen-Heravi F: Disruption of monocyte and macrophage homeostasis in periodontitis. Front Immunol 11: 330, 2020.
38. Wang C, Zhao Q, Chen C, Li J, Zhang J, Qu S, Tang H, Zeng H and Zhang Y: CD301b+ macrophage: The new booster for activating bone regeneration in periodontitis treatment. Int J Oral Sci 15: 19, 2023.
39. Wang Y, Zhang X, Wang J, Zhang Y, Ye Q, Wang Y, Fei D and Wang Q: Inflammatory periodontal ligament stem cells drive M1 macrophage polarization via exosomal miR-143-3p-mediated regulation of PI3K/AKT/NF-κB signaling. Stem Cells 41: 184-199, 2023.
40. Qian JK, Ma Y, Huang X, Li XR, Xu YF, Liu ZY, Gu Y, Shen K, Tian LJ, Wang YT, *et al*: The CD163/TWEAK/Fn14 axis: A potential therapeutic target for alleviating inflammatory bone loss. J Orthop Translat 49: 82-95, 2024.
41. Winkles JA: The TWEAK-Fn14 cytokine-receptor axis: Discovery, biology and therapeutic targeting. Nat Rev Drug Discov 7: 411-425, 2008.
42. Wang W, Shi X, Feng J, Le Y, Jin L, Lu D, Zhang Q and Wang C: Perinatal exposure to PBEB aggravates liver injury via macrophage-derived TWEAK in male adult offspring mice under western diet. J Hazard Mater 479: 135735, 2024.
43. Liu L, Wu P, Wei Y, Lu M, Ge H, Wang P, Sun J, Horng T, Liu X, Shen X, *et al*: TWEAK-Fn14 signaling protects mice from pulmonary fibrosis by inhibiting fibroblast activation and recruiting pro-regenerative macrophages. Cell Rep 44: 115220, 2025.

44. Vincent C, Findlay DM, Welldon KJ, Wijenayaka AR, Zheng TS, Haynes DR, Fazzalari NL, Evdokiou A and Atkins GJ: Pro-inflammatory cytokines TNF-related weak inducer of apoptosis (TWEAK) and TNFα induce the mitogen-activated protein kinase (MAPK)-dependent expression of sclerostin in human osteoblasts. J Bone Miner Res 24: 1434-1449, 2009.
45. Holmberg R, Robinson M, Gilbert SF, Lujano-Olazaba O, Waters JA, Kogan E, Velasquez CLR, Stevenson D, Cruz LS, Alexander LJ, *et al*: TWEAK-Fn14-RelB signaling cascade promotes stem Cell-like features that contribute to Post-chemotherapy ovarian cancer relapse. Mol Cancer Res 21: 170-186, 2023.
46. Liu W, Gao L, Hou X, Feng S, Yan H, Pan H, Zhang S, Yang X, Jiang J, Ye F, *et al*: TWEAK Signaling-induced ID1 expression drives malignant transformation of hepatic progenitor cells during hepatocarcinogenesis. Adv Sci 10: e2300350, 2023.
47. Ando T, Ichikawa J, Wako M, Hatsushika K, Watanabe Y, Sakuma M, Tasaka K, Ogawa H, Hamada Y, Yagita H and Nakao A: TWEAK/Fn14 interaction regulates RANTES production, BMP-2-induced differentiation, and RANKL expression in mouse osteoblastic MC3T3-E1 cells. Arthritis Res Ther 8: R146, 2006.
48. Zou X, Tian Y, Peng L, Luo M, Yan Z, Xue Z, Liu X and Xia Y: TWEAK regulates the functions of hair follicle stem cells via the Fn14-Wnt/β-catenin-CXCR4 signalling axis. Wound Repair Regen 33: e70032, 2025.
49. Wang Y, Wang L, Sun T, Shen S, Li Z, Ma X, Gu X, Zhang X, Peng A, Xu X and Feng Q: Study of the inflammatory activating process in the early stage of Fusobacterium nucleatum infected PDLSCs. Int J Oral Sci 15: 8, 2023.
50. Wang P, Tian H, Zhang Z and Wang Z: EZH2 regulates lipopolysaccharide-induced periodontal ligament stem cell proliferation and osteogenesis through TLR4/MyD88/NF-κB pathway. Stem Cells Int 2021: 7625134, 2021.
51. Guan XX, Yang HH, Zhong WJ, Duan JX, Zhang CY, Jiang HL, Xiang Y, Zhou Y and Guan CX: Fn14 exacerbates acute lung injury by activating the NLRP3 inflammasome in mice. Mol Med 28: 85, 2022.
52. Zhao Y, Quan Y, Lei T, Fan L, Ge X and Hu S: The role of inflammasome NLPR3 in the development and therapy of periodontitis. Int J Med Sci 19: 1603-1614, 2022.
53. Mao H, Gong T, Sun Y, Yang S, Qiao X and Yang D: Bacterial growth stage determines the yields, protein composition, and periodontal pathogenicity of porphyromonas gingivalis outer membrane vesicles. Front Cell Infect Microbiol 13: 1193198, 2023.
54. Liang F and Huang S: PGC-1α inhibits NLRP3 signaling through transcriptional activation of POP1 to alleviate inflammation and strengthen osteogenic differentiation of lipopolysaccharide-induced human periodontal stem cells. Prostaglandins Other Lipid Mediat 174: 106853, 2024.
55. Michaelson JS and Burkly LC: Therapeutic targeting of TWEAK/Fn14 in cancer: Exploiting the intrinsic tumor cell killing capacity of the pathway. Results Probl Cell Differ 49: 145-160, 2009.
56. Roessler M, Vega-Harring SM, Jarutat T, Geho D, Wang K, DeMario M, Goss GD and Schellens JH: Exposure and tumor Fn14 expression as determinants of pharmacodynamics of the Anti-TWEAK monoclonal antibody RG7212 in patients with Fn14-positive solid tumors. Clin Cancer Res 22: 858-867, 2016.
57. Alvarez de Cienfuegos A, Cheung LH, Mohamedali KA, Whitsett TG, Winkles JA, Hittelman WN and Rosenblum MG: Therapeutic efficacy and safety of a human fusion construct targeting the TWEAK receptor Fn14 and containing a modified granzyme B. J Immunother Cancer 8: e001138, 2020.
58. Keshtvarz M, Rezaei E, Amani J, Pourmand MR, Salimian J, Sarial S and Douraghi M: A novel shiga based immunotoxin against Fn-14 receptor on colorectal and lung cancer. Int Immunopharmacol 110: 109076, 2022.
59. Schneider CS, Perez JG, Cheng E, Zhang C, Mastorakos P, Hanes J, Winkles JA, Woodworth GF and Kim AJ: Minimizing the non-specific binding of nanoparticles to the brain enables active targeting of Fn14-positive glioblastoma cells. Biomaterials 42: 42-51, 2015.
60. Guerrero-Hue M, Vallejo-Mudarra M, García-Caballero C, Córdoba-David GM, Palomino-Antolín A, Herencia C, Vendrell-Casana B, Rubio-Navarro A, Egido J, Blanco-Colio LM and Moreno JA: Tweak/Fn14 system is involved in rhabdomyolysis-induced acute kidney injury. Biomed Pharmacother 169: 115925, 2023.
61. Hotta K, Sho M, Yamato I, Shimada K, Harada H, Akahori T, Nakamura S, Konishi N, Yagita H, Nonomura K and Nakajima Y: Direct targeting of fibroblast growth factor-inducible 14 protein protects against renal ischemia reperfusion injury. Kidney Int 79: 179-188, 2011.
62. Dou Y, Li C, Li L, Guo J and Zhang J: Bioresponsive drug delivery systems for the treatment of inflammatory diseases. J Control Release 327: 641-666, 2020.